Marine and Petroleum Geology 155 (2023) 106376

Contents lists available at ScienceDirect

Marine and Petroleum Geology

journal homepage: www.elsevier.com/locate/marpetgeo

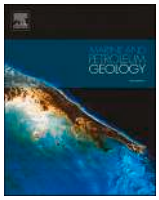

Normal faulting and landsliding in morpho-structural domes related to buried salt stocks, Zagros Mountains, Iran. Insights into salt breakout

Francisco Gutiérrez [a,*], Mehdi Zarei [b], Michael R. Hudec [c], Hosein Deirnik [b]

[a] Department of Earth Sciences, University of Zaragoza, Pedro Cerbuna 12, 50009, Zaragoza, Spain
[b] Department of Earth Sciences, School of Science, Shiraz University, Shiraz, Iran
[c] Bureau of Economic Geology, Jackson School of Geosciences, The University of Texas at Austin, Box X, Austin, Texas, 78713-8924, USA

ARTICLE INFO

Keywords:
Active diapirism
Surface faulting
Growing anticline
Slope collapse
DSGSD
Salt breakout

ABSTRACT

Normal faulting in domal structures above diapirs has important implications in hydrocarbon geoscience, but studies on surface faulting on exposed growing domes are scarce. Moreover, there is limited work addressing the erosional processes involved in the unroofing of active diapirs preceding salt emergence. This investigation analyses two morpho-structural domes (Gavbast Dome: GD; Kooh Bedoo Dome: KBD) associated with growing anticlines related to the rejuvenation of precursor buried salt stocks in the Zagros Mountains. The structural relief of the domes (1330 m in GD and 400 m in KBD) and the available chronological data on fold development indicate long-term uplift rates of around 0.1–0.4 mm/yr. GD displays three domains with different fault patterns: (1) fold-normal grabens in one half; (2) polygonal faulting with multiple enclosed graben depressions in the crest; and (3) fold-parallel faulting on the other half. KBD shows a major fold-normal graben restricted to the crest and one flank of the dome. The lack of the typical radial pattern related to multidirectional hoop extension can be attributed the suppression of extension in the fold-normal direction by regional shortening. Other factors such as complexities in the folding structure, outer-arc extension in the anticline crests, and plan geometry seem to play a local control on fault patterns. The studied domes display an extraordinarily high density of large slope movements, indicating that they play an instrumental role in the unroofing process. The slope failures, with sliding planes mainly developed in argillaceous units overlain by thick limestone packages, include incipient planar rock slides more than 5 km^2 in area expressed as buckle folds in the lower part of the slopes. The main preparatory factors involved in the development of these slope collapses include rock mass weakening by faulting and slope over-steepening, both related to doming. Our detailed mapping and the examination of a number of salt diapirs in the Fars Arc suggest that episodic landsliding and more gradual fluvial dissection, often controlled by grabens, are the main erosional processes involved in the unroofing of active diapirs leading to salt emergence.

1. Introduction

Three styles of diapiric growth can be differentiated (Jackson and Hudec, 2017): (1) *reactive diapirism,* when salt flows upward to fill the space created by extension beneath a faulted and thinned overburden; (2) *active diapirism*, when salt rises below an overburden, arching, piercing and shouldering it aside; and (3) *passive diapirism*, when salt emerges at the surface and rises without the restraining effect of a roof. Salt rise in a buried salt stock (active diapirism) causes uplift, arching, and inflation in the roof of the diapir (i.e., doming). The rise of a salt stock with an ideal hemispherical top exerts centrifugal forces on the encasing overburden, tending to inflate it like a balloon. These divergent forces, perpendicular to the top boundary of the salt (Nikolinakou et al., 2014), may produce multidirectional tangential extension in the domal roof (Fig. 1). In brittle sediments, circumferential or hoop extension is accommodated by radial faulting, mostly confined to the area of arched overburden. Hoop extension is proportional to plan-view curvature of the diapir, and consequently the frequency of radial faults increases in the sectors with higher curvature (Link, 1930; Parker and McDowell, 1951; 1955; Cloos, 1955, 1968; Withjack and Scheiner, 1982; Schultz-Ela et al., 1993; Stewart, 2006; Yin and Groshong, 2007; Sims et al., 2013). Radial extension tends to produce a graben in the dome crest bounded by an enclosed inward-dipping polygonal or circular fault (i.e., apical conical graben) (McDowell, 1951; Schmidtz and Flizeder, 1993;

* Corresponding author.
E-mail address: fgutier@unizar.es (F. Gutiérrez).

https://doi.org/10.1016/j.marpetgeo.2023.106376
Received 5 May 2023; Received in revised form 9 June 2023; Accepted 11 June 2023
Available online 24 June 2023

Alsop, 1996; Davison et al., 2000; Yin and Groshong, 2007; Stewart, 2006; Dooley et al., 2015). Substantial deformation may occur in this crestal graben to fill the concentric extensional gap generated between the downthrown block and the surrounding flaps (Yin and Groshong, 2007). Radial and concentric normal faults roughly trend parallel and perpendicularly to the dip of the domed strata, respectively. These two sets of faults can intersect and mutually offset to form a polygonal fault system in the crestal zone of the diapir's roof (Gaullier and Vendeville, 2005; Yin and Groshong, 2007; Sims et al., 2013; Clausen et al., 2014). Natural examples and experimental models indicate that radial faulting is the most common fault pattern in the roof of subcircular salt stocks and pillows, and that the less frequent crestal grabens commonly occur at advanced stages of doming and uplift (Parker and McDowell, 1955; Withjack and Scheiner, 1982). Radial faults compartmentalize trapezoidal overburden blocks that separate circumferentially and rotate radially upward and outward. Both hoop extension and uplift decrease outward, and consequently the vertical and horizontal separation of the resulting supra-salt faults diminishes laterally from the crest to zero at the outer edge (annular hinge line) of the dome (Stewart, 2006; Yin and Groshong, 2007). Differential rotation in these compartments results in the development of trapezoidal grabens, half-grabens, and horsts.

In compressional environments such as collisional orogens, precursor salt stocks are commonly located in the core of anticlines, functioning as weak zones that control the initiation and lateral propagation of anticlines (i.e., strain enhancers and localizers) (e.g., Callot et al., 2007; Jahani et al., 2009). Buckling folding related to far-field forces amplifies and tightens the anticlines. This folding mechanism is accompanied by outer-arc extension in the crestal zone, which tends to produce fold-parallel normal faults. The amount of extension in these tangential-strain faults decreases downwards. Anticline contraction is accompanied by convergence in the walls of the associated salt stocks (i.e., displacement loading), forcing the squeezed salt to flow vertically, mainly towards the surface, inducing contractional active rise. Scaled physical models of buried stocks affected by lateral shortening reveal that salt can flow: (1) inward/upward into the diapir from the source layer feeding the stock; and (2) outward/downward into the pedestal and source layer, depleting the stock and causing uplift in the vicinity. This latter downward salt expulsion from the squeezed stock (salt export) commonly occurs during advanced stages of shortening and is favored by a thick and resistant roof and a thick source layer (Dooley et al., 2009, 2015).

The roof of an inflating salt stock located in the core of an anticline affected by regional shortening is subject to two main stress fields: (1) local and multidirectional centrifugal forces imposed by the pressurized salt, squeezed by contractional loading; and (2) regional fold-normal compression (Fig. 1). Moreover, the hinge zone of tightly folded anticlines can experience bending-related out-arc extension, resulting in the development of normal faults parallel to the fold axis. In the shortening direction, the outward extensional forces related to diapiric inflation may be suppressed by inward regional compression. The resulting local stress field in the diapir roof would be one dominated by fold-parallel extension that produces normal faults parallel to the shortening direction (Withjack and Scheiner, 1982; Sims et al., 2013). Withjack and Scheiner (1982), using an experimental physical model (clay layer domed by an underlying inflated balloon), investigated surface fault patterns developed on circular and elliptical domal structures affected by simultaneous local inflation and regional compression. They found that normal faults in the crest and flanks predominantly strike parallel to the compression direction, rather than showing a radial pattern. They also observed minor strike-slip faults trending 30° from the compression direction in the flanks, and small-offset reverse faults perpendicular to the compression direction in the peripheral areas. The main difference observed in domes with elliptical outline was that normal faults parallel to the compression direction curve outward towards the ends of the long axis of the diapir controlled by the higher curvature of the dome edge (see fiigure 17 in Withjack and Scheiner, 1982). In contrast, in the absence of regional stresses, normal faults developed in ellipsoidal domes were dominantly parallel to the major axis of the dome and concentrate in the crestal zone.

The uplift rate in morpho-structural domes overlying salt stocks affected by contractional loading is controlled by a number of factors related to the driving and restraining forces (Nilsen et al., 1995;

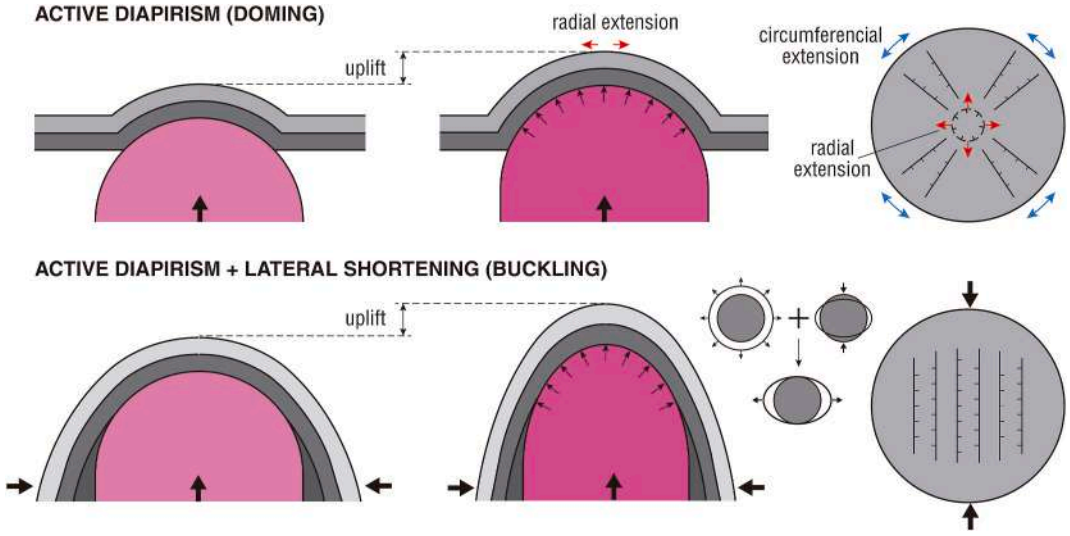

Fig. 1. Patterns of normal faults developed in the roof of actively rising salt stocks with circular outline. Top: Salt rise without the interplay of regional stresses causes doming and inflation in the overburden. Circumferential or hoop extension produces radial normal faults, while radial extension may generate enclosed grabens in the crestal zone bounded by inward-dipping circular or polygonal faults. Bottom: In a rising stock located in the core of an anticline affected by regional shortening (buckling), lateral compressional forces superimpose on the multidirectional forces related to diapirism, fostered by displacement loading. As illustrate the strain ellipses, far-field compressional forces tend to suppress the outward expansion forces induced by diapirism in the shortening direction, resulting in the development of normal faults parallel to the shortening direction (i.e., transverse faults roughly perpendicular to the fold axis). Variations in the fault pattern can be expected depending on the plan-view (circular versus elliptical) and cross-sectional (flat-topped versus rounded) geometry of the stock, the relative importance of the local (multidirectional) and regional (directional) stresses, the presence of pre-existing anisotropies (e.g., fractures) in the overburden, and the degree of lateral confinement in the morpho-structural dome.

Vendeville and Nilsen, 1995; Jackson and Hudec, 2017): (1) salt supply from the source layer and its potential depletion and welding; (2) rate of convergence of the stock walls and share of upward and downward flow of the squeezed salt stock; (3) diameter of the stock, which determines the sectional area of the vertical channel through which the salt flows, decreasing as the stock contracts; (4) weight and strength of the roof, which may be affected by erosional unroofing and weakened by faulting. Eventually, the walls of the stock can be pinched off, disconnecting the upper part of the diapir (teardrop diapir) from the pedestal and the source layer. At a more advanced stage of contraction, the stock can be transformed into a complete secondary weld. This processes requires intense shortening in the country rock surrounding the convex-outward walls of the stock (Jackson and Hudec, 2017).

Diapiric inflation and contractional buckling in the roof of actively rising salt stocks associated with growing anticlines produces: (1) rock uplift and potentially increase in local relief; (2) the steepening of the dip of the strata and the slopes; and (3) weakening of sediments by faulting and bedding-parallel flexural-slip. The first two factors contribute to increase the gravitational shear stresses, while the third factor reduces the shear strength of potential failure planes and creates discontinuities that may function as release and breakout planes for landslide development. This diapiric-tectonic scenario, commonly accompanied by large earthquakes, favors the development of landslides, particularly massive planar slides detached along weak units or stratigraphic discontinuities (Gutiérrez et al., 2023). Once the overburden has been pierced and/or truncated by erosion, the salt may extrude at the surface and function as a passive diapir, eventually feeding a salt sheet (namakier). Physical models suggest that salt initially extrudes at sites where the overburden has been thinned and weakened by landslides and radial faulting (Dooley et al., 2009, 2015).

Normal faulting in the roof of salt stocks and salt pillows has received considerable attention in the international literature because of their practical implications for exploration and development of hydrocarbons. *Roofs above salt structures typically form anticlinal closures, so are highly prospective hydrocarbon traps. These traps can be complicated by the presence of crestal normal faults, which can segment the traps if the faults seal, or cause them to leak if the faults transmit fluids (Sims et al., 2013).* Published works modelling crestal faults are mainly focused on scaled physical models and numerical models, referred to above. These models explore faulting in rather homogenous diapir roofs lacking pre-existing fractures and located in virtual settings lacking structural complexity. In contrast, published investigations dealing with well-exposed normal faults developed in lithified strata above buried stocks are very scarce (Davison et al., 1996; Almalki et al., 2015). *A key to predicting the geometries and sealing properties of these crestal normal faults is understanding their genesis. Field studies such as this one can offer important insights to modeling and de-risking prospects associated with crestal anticlines.*

In this work we analyze normal faults and large landslides developed in two morpho-structural domes associated with buried salt stocks located in the core of growing anticlines affected by contractional loading. The selected sites in the Fars Arc of the Zagros Mountains provide an excellent opportunity to expand our knowledge on the following aspects related to active diapirism: (1) surface-fault patterns developed in lithified roofs of buried salt stocks located in a compressional environment; (2) potential influence of structural complexities and overburden anisotropies on normal faulting; (3) processes that participate in the mechanical weakening and erosional unroofing of domes underlain by rising salt stocks, eventually leading to the onset of passive diapirism (i.e., salt emergence). Salt extrusions in the Zagros Mountains have been the focus on numerous publications addressing multiple aspects (e.g., Talbot and Pohjola, 2009; Zarei et al., 2012; Jahani et al., 2017; Závada et al., 2021 and references therein), but to our knowledge this is the first work dealing specifically with domes associated by buried salt stocks.

The Zagros Fold-and-Thrust Belt hosts around 8% and 15% of the global oil and gas reserves, respectively. Most of the oil has accumulated in the Asmari Fm. (75%) and the Bangestan Group. The oil was sourced from the Pabdeh and Kazhdumi formations, migrated upwards to carbonate formations since the onset of the Zagros Folding, and was trapped in structural highs sealed by impervious marls (e.g., Pabdeh Fm.) and evaporites (Gachsaran Fm.) (Bordenave and Hegre, 2010). The rocks exposed in the analyzed domes show the classical stratigraphic succession of the Fars Arc (described below; see Jahani et al., 2009), including the prolific carbonates of the Asmari Fm. and the Bangestan Group, although no oil reservoirs seem to occur in the area (Bordenave and Hegre, 2010). Some anticlines west of the analyzed sector host prolific gas reservoirs in Permo-Triassic carbonate formations (Dalan and Kangan Fms.) sealed by the anydritic Dahtak Formation of Triassic age. The source for these gas reservoirs is ascribed to Silurian organic-rich shales. However, it seems that the analyzed area did not functioned as an accumulation zone during the long-range migration of the gas before the Zagros folding (Bordenave and Hegre, 2010).

2. General geological setting

The NW-SE oriented Zagros Fold-and-Thrust Belt, on the northeastern margin of the Arabian Plate, results from the closure of the Neo-Tethys ocean and the Cenozoic collision between the Arabian and Eurasian plates (Fig. 2). According to GPS data, the plates are currently converging along a general N-S direction at a rate of 20–25 mm/yr, of which around one third is accommodated within the Zagros Belt (Vernant et al., 2004). This orogenic system is divided into two main longitudinal structural zones (Fig. 2): (1) the High Zagros (or Imbricated Belt) on the NE; and (2) the Simply Folded Belt on the SW. The High Zagros is bounded by the High Zagros Fault on the SW and the Main Zagros Reverse Fault on the NE, considered as the suture between the Arabian and Eurasian plates (Stöklin, 1968). The Simply Folded Belt is located between the High Zagros Fault and the SE-propagating Zagros Deformation Front, which defines the edge of the current foreland basin associated with the Persian Gulf and the Mesopotamian Plain. The Simply Folded Belt comprises three domains with distinctive stratigraphic and structural features (i.e., different detachment horizons) bounded by major oblique N-S and E-W striking fault zones, from NW to SE (Motiei, 1993; Sepehr and Cosgrove, 2004): (1) the Lurestan Arc; (2) the Dezful Embayment; and (3) the Fars Arc, between the right-lateral Kazerun-Borazjan Fault system and the Oman Line (or syntaxis). Here, the main detachment corresponds to the highly mobile 1–1.5 km thick Hormuz salt of Neoproterozoic-Cambrian age (Talbot and Alavi, 1996).

The Fars Arc displays an arcuate system of folds, which trend changes towards the SE from the typical NW-SE Zagros grain to an ENE-WSW orientation (Fig. 3). The structural style is dominated by detachment folds, decoupled from the basement along the Hormuz salt, situated at a depth of 11–15 km (Jahani et al., 2009). Shortening in the basement is chiefly accommodated by blind N- to NE-dipping reverse faults, capable of producing major earthquakes, but rarely accompanied by surface ruptures because the thick Hormuz salt functions as a barrier for fault propagation (Berberian, 1995, 2014; Nissen et al., 2011). The folds in the western and central-eastern sectors of the Fars Arc are punctured by numerous extrusions of Hormuz salt (passive diapirism) at various evolutionary stages, including growing domes, salt fountains with a summit dome, degrading salt droplets and domes, and flat-floored craters (Jahani et al., 2007, 2009; Talbot and Pohjola, 2009; Mukherjee et al., 2010; De Waele and Gutiérrez, 2022). Some anticlines locally display superimposed domal structures related to buried salt plugs with inflated roofs that have not emerged at the surface yet (active diapirism), like the ones investigated in this work (Fig. 3). Most of the salt diapirs in the Zagros were initiated long before the current orogenic stage and have experienced rejuvenation by displacement loading (i.e., squeezing) during the Cenozoic collision (Harrison, 1930; Kent, 1979; Jahani et al., 2007, 2009 and references therein). Passive and active diapirism during pre-orogenic times is recorded by: (1) Hormuz-derived debris in sediments deposited by allocthonous salt sheets in the

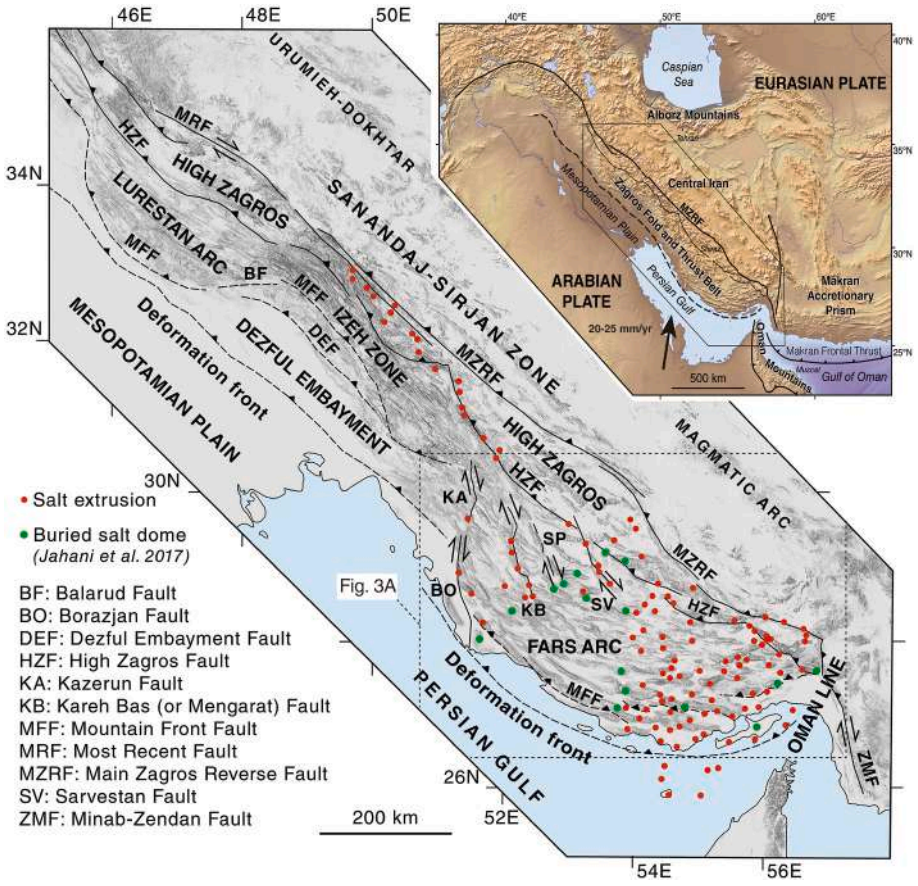

Fig. 2. Geotectonic setting of the Zagros Fold-and-Thrust Belt, related to the ongoing collision between the Arabian and Eurasian plates, and sketch of the Zagros orogen showing the structural zones, the main faults and the distribution of salt extrusions and buried salt plugs.

surroundings of salt extrusions; (2) thickness and facies variations, hiatuses, and growth strata in syn-kinematic sediments associated with the diapirs. In the western sector of the Fars Arc, oblique plate convergence and differential shortening between the Fars salient and the Dezful re-entrant is accommodated by dextral displacement along outcropping N-S faults with associated salt extrusions (Talbot and Alavi, 1996; Walpersdorf et al., 2006; Tavakoli et al., 2008; Authemayou et al., 2009; Jahani et al., 2017). In the central sector, where the analyzed domes are located, the strike-normal plate displacement results in pure shortening (Walpersdorf et al., 2006; Tavakoli et al., 2008) (Fig. 3).

3. Methodology

This work is essentially based on detailed geological-geomorphological mapping of the domal structures associated with buried salt stocks and field surveys. Mapping, covering a total area of 1200 km^2, was conducted following a phased approach. Firstly, preliminary maps were drafted through the interpretation of the following spatial data: (1) grey-scale stereoscopic aerial photographs from 1956 printed at an approximate scale of 1:40,000; (2) shaded relief models derived from TanDEM-X DEMs (2014) with a spatial resolution of 12 m; (3) satellite images from GoogleEarth with spatial resolution better than 5 m; and (4) the 1:250,000 scale South-East Fars Geological Compilation Map (Perry et al., 1965). The TanDEM-X DEMs (German Aerospace Center; DLR), derived from bistatic X-Band inteferometric SAR data acquired by the satellites TanDEM-x (TDX) and TerraSAR-X (TSX) have absolute and relative vertical accuracies of <10 m and 2–4 cm, respectively (Wessel, 2016). In a subsequent stage, we conducted field surveys in the critical sectors using satellite images uploaded in a tablet with a GPS sensor (3–5 m horizontal accuracy). Field work allowed us to improve the preliminary maps, examine and photograph key geological features, collect structural data, and construct topographic profiles across fault scarps using a laser rangefinder (Nikon Forestry Pro). The TanDEM-X DEMs were used to extract topographic and morphometric data using a GIS. Landslide volumes have been roughly estimated using cross sections constructed with TanDEM-X DEMs and the geological maps and assuming planar bedding-controlled sliding surfaces for the non-rotational slope movements.

4. Gavbast Dome

4.1. Geology & geomorphology

The Gavbast Dome is located in the southern-central sector of the Fars Arc, relatively close to the current Deformation Front (Fig. 3). This prominent morpho-structural dome is centered along the axis of a major E-W to WNW-ESE anticlinal structure, providing evidence for a buried salt stock in the anticline core. The Gavbast Dome occurs where the 75 km long and sinuous Gavbast Anticline splays to the west into two narrow anticlines; the 50 km long Bayram Anticline and the 130 km long Varavi Anticline to the N and S, respectively. Consequently, the fold at Gavbast displays contrasting along-strike geometry, with a broad and relatively planar west-plunging synclinal pericline on the western side and an antiformal structure on the eastern side (Figs. 3 and 4). Gutiérrez et al. (2023) proposed that the long anticlinal ridge associated with the Gavbast Dome is probably underlain by a seismogenic, N-dipping, reverse basement fault. The following lines of evidence support the presence of such blind fault, likely decoupled from the Phanerozoic cover by the Hormuz salt: (1) asymmetric geometry of the anticlinal structure with steeper southern limb; (2) significant down-to-the-south

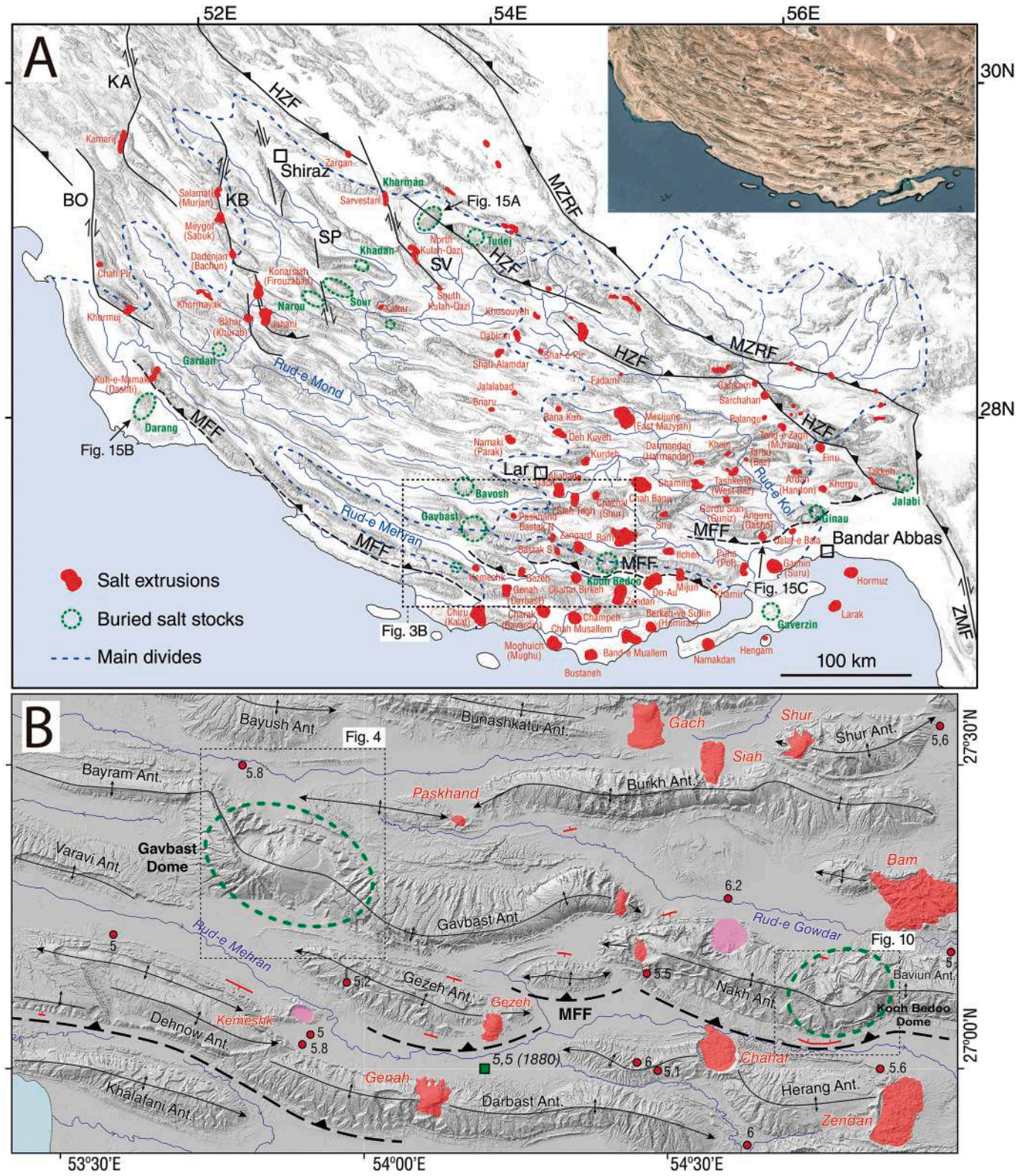

Fig. 3. The Fars Arc and the setting of the analyzed domes. (A) Map of the Fars Arc of the Simply Folded Belt showing the salt extrusions and buried salt stocks indicated by Jahani et al. (2017). The main watershed divides and drainage network are depicted. (B) Hillshade showing the distribution of anticlinal ridges, salt extrusions (red) and diapiric craters (pink; vanished salt extrusions) in the vicinity of the Gavbast and Kooh Bedoo domes (green dashed ellipses). The N-dipping Mountain Front Fault (MFF; blind basement reverse fault) inferred by Berberian (1995) is indicated with a dashed trace. Red lines with hachures indicate areas with alluvial fans offset by Quaternary flexural-slip faults related to active folding. Epicenters from the historical catalog of Berberian (2014) (green squares, estimated M_s magnitude) and the instrumentally recorded events with $M_s \geq 5$ (red circles) from Berberian's catalog (1900–2005) and that of the Iranian Seismological Center (2006–2022). Number of people killed in the 1880 Jonah (or Jenah) and 1956 Gowdeh earthquakes indicated within an ellipse. The meizoseismal area of the latter event from Berberian (1995) is indicated with a dashed line. Hillshade generated with TanDEM-X DEMs from the German Aerospace Center.

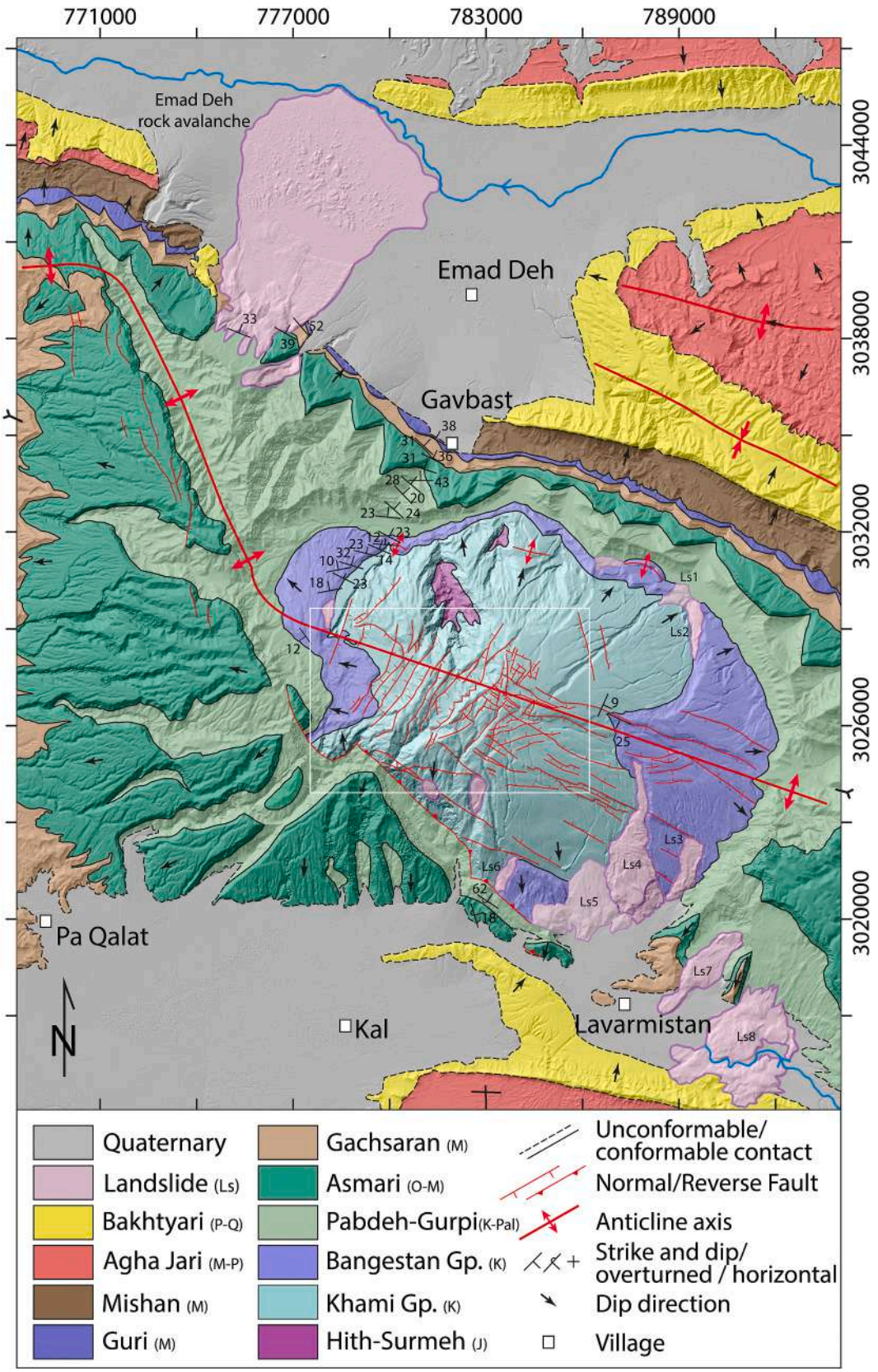

Fig. 4. Geological map of Gavbast Dome related to a buried salt stock in the core of Gavbast Anticline. The dome shows a horst and graben morphostructure controlled by fold-normal faults on the NW portion, and a half-dome geometry in the remaining sector with multidirectional faults. The area shows high density of large landslides developed on stratigraphic successions over-steepened and weakened by diapiric uplift and deformation. The location of the cross-section depicted in Fig. 5 is indicated at the lateral edges of the map. The white rectangle indicates the area covered by Fig. 6. P: Pliocene; M: Miocene: O: Oligocene; Pal: Paleogene; K: Cretaceous; J: Jurassic.

topographic drop across the anticline of ca. 300 m; (3) rare exposures of old formations; (4) the main drainage divides in the Fars Arc (Rud-e Mand, Rud-e Mehran and Rued-e Shur) either coincide with the crest of the anticlinal ridge or meet at Gavbast Dome (Fig. 3); and (5) the ridge displays spatial clusters of huge and potentially coseismic, bedrock landslides, including the 420 Mm^3 Emad Deh rock avalanche (Fig. 4). In the Fars Arc, large-magnitude ($M_w > 6.5$) reverse fault earthquakes occur associated with this type of folds, geometrically distinct from the typical symmetric folds of the Simply Folded Belt (Berberian, 1995; Nissen et al., 2011). Gutiérrez et al. (2023) estimated a minimum long-term uplift rate for the Gavbast Anticline in the vicinity of Gavbast Dome of 0.4–0.7 mm/yr, considering: (1) the elevation difference between the anticlinal ridge and the adjacent synclinal valleys (1170 m and 1430 m to the N and S), which provides a minimum measure of folding-related uplift reduced by erosion in the anticline crest and aggradation in the synclinal basin; and (2) that the time-transgressive basal unconformity of the conglomeratic Bakhtyari Formation records the onset of the morphogenetic folding, which has been dated by magnetostratigraphy at 3-2 Ma at the frontal sector of the Simply Folded Belt (Lurestan Arc; Homke et al., 2004). This chronological constrain is consistent with the age of ca. 3.2 Ma ascribed by magnetostratigraphic studies to the base of the Bakhtiary Fm. in Central Fars, 70 km north of Gavbast (Ruh et al., 2014).

The stratigraphic formations exposed in the mapped area include, in ascending order (Perry et al., 1965; NIOC, 2004a) (thicknesses based on our mapping and cross sections) (Fig. 4): (1) Jurassic-age dolomites of the Surmeh Fm. and anhydrite of the Hith Mb. (2) Early Cretaceous rocks of the Khami Group, comprising the Fahlyan Fm. (limestone), the Gadvan Fm. (shales) and the Dariyan Fm. (limestone). The Jurassic and Early Cretaceous successions ca. 660 m thick (NIOC, 2004a). (3) Early Cretaceous marls and shales of the Kazhdumi Fm. (4) Early-Late Cretaceous Bangestan Group, including limestones of the Sarvak Fm. and the Ilam Fm. The thickness of the landslide-prone stratigraphic packages 3 and 4 based on cross sections is around 130 m, both lumped in our mapping as Bangestan Group. (5) Around 750 m of Late Cretaceous and Paleogene marls with limestone intercalations of the Gurpi and Pabdeh formations. (6) The highly resistant Oligocene-Early Miocene Asmari Limestone. (7) The regressive synorogenic succession of the Fars Group, comprising marine evaporites of the Gachsaran Fm. (Miocene), shallow marine marls of the Mishan Fm. (Miocene), limestone of the Guri Mb. (Miocene), and marls and sandstone of the Agha Jari Fm. (Mio-Pliocene) deposited in transitional environments. (8) The Fars Group is overlain by the continental coarse-grained Bakhtyari Fm., which time-transgressive basal unconformity is considered to record the onset of the most vigorous phase of folding that propagated progressively towards the Deformation Front (Hessami et al., 2001; Vergés et al., 2019).

Gavbast mountain shows an inflated domal morpho-structure superimposed on the Gavbast Anticline. The dome has an elliptical geometry 22 km long and 15 km wide, with its major axis coinciding with the axis of Gavbast Anticline. The vertical uplift and lateral expansion of the overburden (i.e., inflation or doming) above the rising salt stock is recorded by the following structural and geomorphic features (Figs. 4 and 5): (1) local variations in the strike and dip of bedding, notably dip oversteepening related to upward and outward rotation of strata; (2) widening of the anticline, particularly on the gentler northeastern limb, where the stratigraphic units show a clear outward deflection of around 1.8 km (Figs. 3B and 4); (3) reverse faulting associated with the southwestern edge, where the anticline has a steeper and locally overturned limb; (4) upward bulging of the anticline crest; (5) normal faulting with conspicuous geomorphic expression; and (5) abundant bedding-controlled landslides. The dome displays two contrasting morpho-structural domains. The NW sector shows a transverse horst and graben topography, while the remaining portion exhibits a half-dome morphology (Fig. 4). The concordant half-dome topography is essentially controlled by resistant limestone units exhumed by differential erosion at the top of the Khami Group (Dariyan Fm.) and the Bangestan Group (Sarvak and Ilam Fms.). The well-preserved structural surface on top of the Khami Group is largely underlain by a hardground on fossiliferous limestone (lumachelle) strongly indurated by carbonate and iron oxide cementation. The dip slope developed on the top of the Bangestan Group forms a large and convex flatiron on the SE pericline of the dome.

The longitudinal cross-section constructed along the axis of the fold and dome reveals a bulge ca. 1300 m high in the crest of the Gavbast Anticline related to diapiric deformation (Fig. 5). Assuming that: (1) diapiric uplift of the Cretaceous formations has occurred during the orogenic phase; and (2) the doming process started coevally with the onset of the morphogenetic folding, recorded by the basal unconformity of the Bakhtyari Fm. at ca. 3-2 Ma, we can tentatively estimate a local diapiric uplift rate of 0.43–0.65 mm/yr. The actual value could be lower due to possible pre-orogenic uplift of the diapir roof (Jahani et al., 2009) and the initiation of the diapir rejuventation before the vigorous folding phase. Nonetheless, two processes have contributed to the relief of Gavbast Dome, which is the highest mountain in the region (2137 m a.s.l.), namely folding related to regional shortening and doming caused by the rise of the buried salt stock.

Jahani et al. (2009) constructed a 230 km long geological cross-section traversing the Gavbast Dome based on seismic images, unpublished geological maps of the National Iranian Oil Company, well information and field data. This section depicts a salt stock in the core of the Gavbast Dome roofed by arched Permian to Cretaceous strata and surrounded by Paleozoic formations in discordant diapiric contact with the Hormuz salt. Jahani et al. (2009) indicate that Gavbast Dome can be considered as an exposed analogue to the offshore domal structures present in foreland sectors of the Persian Gulf, some of which host prolific hydrocarbon reservoirs (Edgell, 1996; Sims et al., 2013).

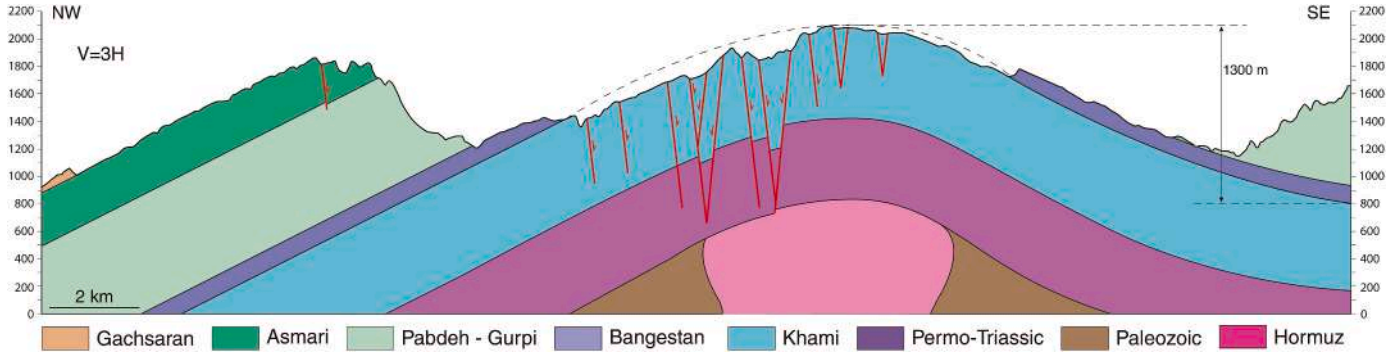

Fig. 5. Longitudinal cross-section along the axis of Gavbast dome and anticline indicating approximate local uplift related to diapiric doming. Thickness of not fully exposed units derived from NIOC (2004a). Trace of section indicated in Fig. 4. Vertical exaggeration x3.

4.2. Normal faults

A total of 126 surface normal faults have been mapped on Gavbast Dome (Figs. 4 and 6). The strike frequency shows a primary mode parallel to the fold axis and a secondary fold-normal mode (see rose diagram in Fig. 6B). Normal faults at Gavbast Dome mostly occur along the axial-crestal zone and the southwest flank. Three domains can be differentiated on the basis of the cartographic fault patterns (Fig. 6): (1) northwest sector; (2) crestal sector; and (3) southeast flank.

The majority of the normal faults on the NW portion of the dome display a NE-SW orientation perpendicular to the axis of Gavbast anticline and elongated dome. These fold-normal faults have formed two transverse grabens and an intervening horst that disrupt the overall domal geometry of the mountain (Figs. 5 and 6). The upper SE graben, 3.9 km long and 1.2 km wide, shows a tapered geometry in plan and an asymmetric cross-section, with a master normal fault on the SE margin and a staircase controlled by three antithetic faults on the opposite margin (Fig. 7). The bottom of the graben depression displays limited dissection and aggradation. The topographic relief of 240 m associated with the SE margin of the graben can be considered as a good approximation to the throw of the master fault. The elevation difference between the graben floor and the horst on the NE margin is around 110 m.

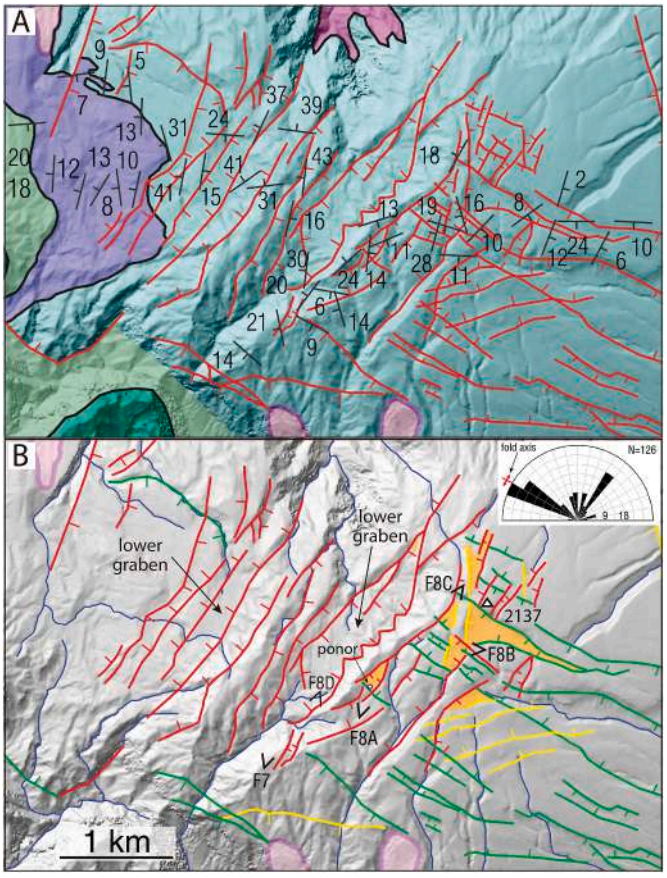

Fig. 6. Detailed maps of the sector with highest density of normal faults. (A) Map including strike and dip data. The NW sector of the dome displays two transverse grabens separated by an intervening horst. The crestal sector shows a polygonal fault system related to the superposition of transverse, longitudinal and oblique (i.e, perpendicular to dip of strata) faults. (B) Map showing the distribution of the main drainage network and fault groups: transverse (red), longitudinal (green), and oblique (yellow). Orange polygons indicate the floor of internally drained polygonal grabens. The triangle indicates the location of the summit. Inset rose diagram indicates the strike frequency of normal faults, showing two clear orthogonal modes. Location of capture points of photographs in Figs. 7 and 8 indicated by Fx.

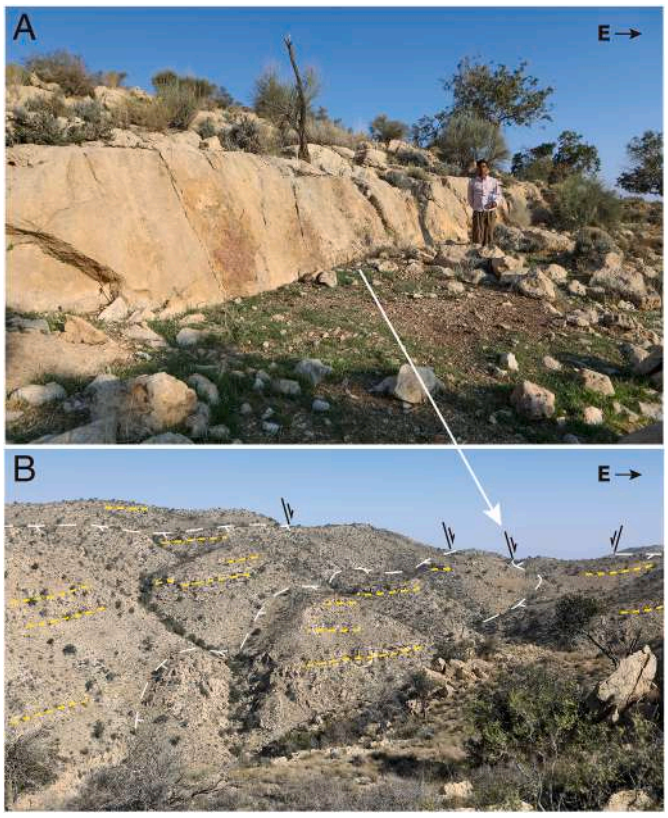

Fig. 7. Images of the transverse SE graben in the NW sector of Gavbast Dome. See location of capture points in Fig. 6B. (A) Exposure of normal fault plane with striations indicating dip-slip displacement, most probably exhumed by differential erosion. Person 1.7 m high for scale. (B) Sequence of SE-dipping normal faults and downthrown blocks in the NE margin of the graben, with a cumulative throw of around 240 m (39R 781489, 3026753).

Nonetheless, the vertical offset across the graben is rather limited (<40 m), considering the general topographic drop to the NW of the domal morpho-structure. The strata in the lower downthrown block shows an asymmetric synformal structure, with steeper beds associated with the master fault dipping around 30°. The high dip of the strata is expressed by the normal fault with serrated pattern and flatirons in the downthrown block (Fig. 6). This is probably a bending structure related to the collapse of a downward-tapering keystone graben. The horst has a limited width of 350–250 m and is underlain by subhorizontal to gently dipping strata. The lower NW graben is around 3.6 km long, 1.3 km wide, and is controlled by five main parallel faults. The floor of the graben shows limited dissection and aggradation. The topographic and structural throw associated with the two main faults on the SE margin is around 200 m. Vertical offset across this graben seems to be very limited. The exposed beds in the downthrown block associated with the master fault also show a relatively high dip towards the graben axis, defining an asymmetric synform (Fig. SM1 in Supplementary Material).

The crestal sector of the dome displays the superposition of three main fault sets forming a polygonal horst and graben morphostructure. These include fold-normal faults, fold-parallel faults, and multidirectional antithetic (i.e., dip opposite to that of the bedding) and synthetic faults striking perpendicularly to the dip the strata up to 2 km long (Fig. 6). This complex fault system has formed enclosed graben depressions bounded by inward dipping faults (Fig. 8). The topographic-structural throw of the largest and deepest one, 1.5 km long covering 0.25 km^2, reaches around 70 m. A triangular depression located next to the NE-facing escarpment of the half-dome displays a swallow hole at the foot of a marginal fault scarp (Fig. 8A). This sink is probably related to a concealed and dilated normal fault with significant horizontal

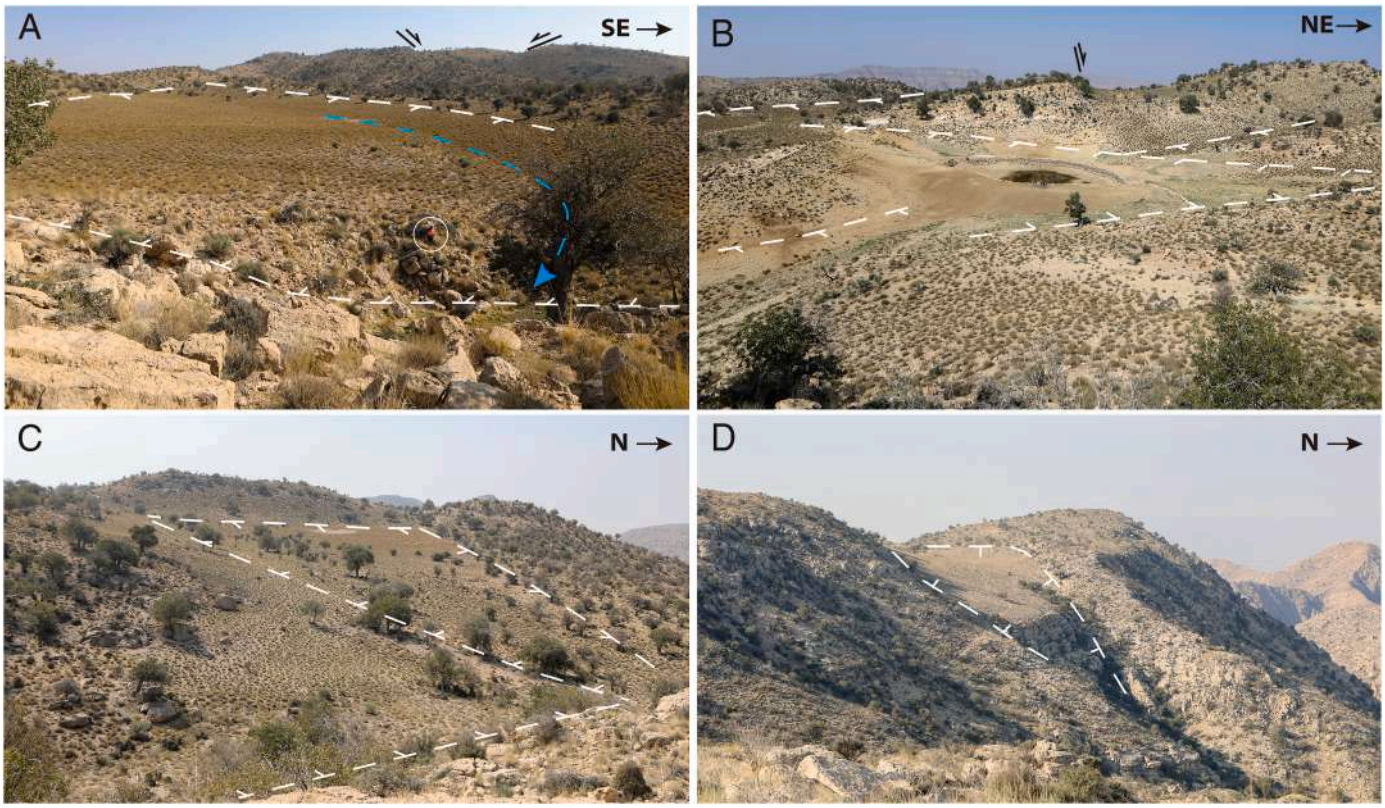

Fig. 8. Images of enclosed grabens related to polygonal faulting in the crestal zone of Gavbast Dome. See location of capture points in Fig. 6B (A) Triangular graben with a swallow hole (ponor) at the foot of a basin-bounding fault scarp (39R 782439, 3026362). (B) Enclosed depression associated with an intersecting system of orthogonal normal faults (39R 783651, 3026598). (C) Triangular graben bounded by rather degraded fault scarps. Location of images shown in Fig. 6B (39R 783460, 3027276). (D) Keystone graben with clear geomorphic expression on the dome crest and SE margin of the upper graben (39R 781402, 3025531).

separation. This depression falls within the category of neotectonic poljes, inasmuch as it is an internally drained basin in carbonate bedrock created by subsidence accommodated by dip-slip faults (De Waele and Gutiérrez, 2022). The following lines of evidence indicate that the scarps surrounding the depressions correspond to normal fault scarps: (1) available exposures either show the faults or reveal different stratigraphic units, often with differing dips, juxtaposed by fault contact; (2) the scarped margins of the depressions are rectilinear and can be locally ascribed to faults associated with exposures; (3) the creation of polygonal enclosed depressions in this setting can only be explained by surface faulting (i.e., differential erosion is not a feasible mechanism).

The SE flank of the dome displays a swarm of fold-parallel faults well expressed in limestone outcrops of the Khami and Bangestan groups and with throws of up to a few tens of meters. This longitudinal fault set includes a conspicuous 8.5 km long and 1.6 km wide graben, running from to crest to the edge of the Gavbast Dome, along its axis (Fig. 4). The vertical separation on these faults decreases toward the edge of the dome.

The drainage network in Gavbast Dome shows an overall radial pattern, with a greater degree of entrenchment in the NW portion (Figs. 4 and 6). Here, the most deeply incised stream is controlled by the SE graben (Fig. 7B). The low-gradient crestal sector of the dome displays a number of internally drained graben depression that have not been captured by the headward-propagating drainage net. The faults in Gavbast Dome show clear geomorphic expression, but the lack of fresh scarps and drainages disrupted by surface ruptures (e.g., defeated streams, beheaded streams, wind gaps) suggest relatively slow slip rates.

4.3. Landslides

The Gavbast Dome and its vicinity displays an extraordinary spatial cluster of landslides, including several slope movements with volumes >100 Mm^3. The foot of the dip slopes on the NE flank of the dome shows peculiar gravitational slope deformation affecting limestones of the Bangestan Group (Sarvak and Ilam Fm.) and the underlying shales and marls of the Kazhdumi Fm. (both lumped as Bangestan Group in the map; Fig. 4). The localized slope failures are expressed as detachment buckle folds with concordant topography, forming anticlinal ridges and synclinal troughs (Fig. 9A and B; Fig. SM2 in Supplementary Material). The folding structures are interpreted as planar slides in which the pinned displaced mass has not lost coherence and has experienced buckle folding in the lower part. The sliding surface is controlled by the extremely planar contact between the top of the Khami Group (strongly indurated limestone) and the mechanically weak argillaceous rocks of the Kazhdumi Fm. The folded slid mass west of landslide Ls1 is 1 km long, 1.4 km wide, covers an approximate area of 0.9 km^2 and occurs on a concordant slope where the strata dip 19° (Fig. 9B). The lower portion of the slope displays two curved anticlinal ridges and synclinal troughs with the convexity pointing downslope. The displaced mass has largely buried a valley and deflected a drainage to the north.

The potentially coseismic Emad Deh rock avalanche, dated at ca. 5.4 ka, is located just NW of the domal structure (Gutiérrez et al., 2023) (Fig. 4). The deposit of this long runout (9.3 km long) rock avalanche amounts 420 Mm^3, and the aggregate volume of the subsequent landslides nested between its lateral levees was estimated at 84 Mm^3, summing ca. 500 Mm^3. A number of landslides have been mapped in the lower and medial parts of the slopes of Gavbast Dome, involving the shales of the Kazhdumi Fm. and the overlying limestones of the Bangestan Group (Fig. 4). These are interpreted as planar failures situated at the top of the Khami Group. The displaced masses have largely lost coherence and disintegrated turning into slide-flow type slope movements. Table 1 indicates the main morphometric parameters of the

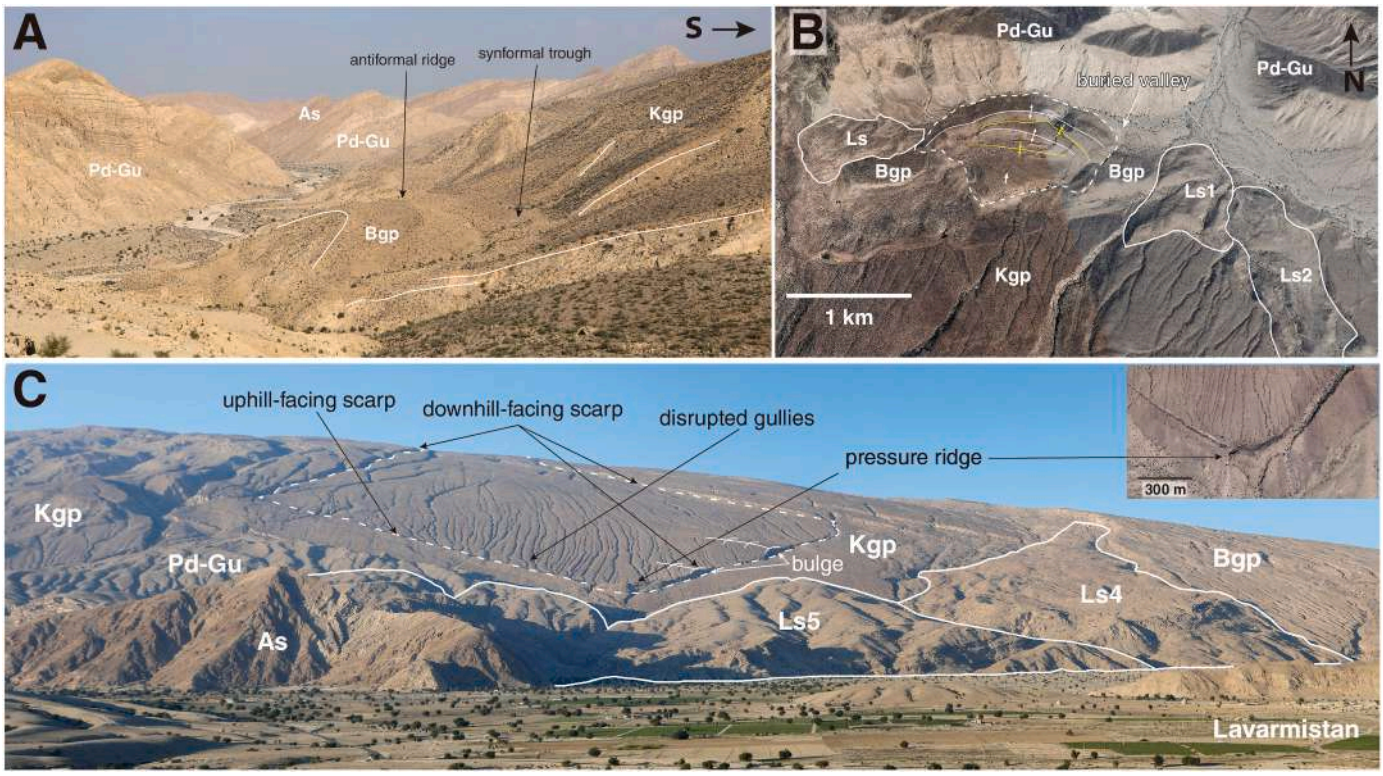

Fig. 9. Images of gravitational slope deformations and landslides in Gavbast Dome. (A) Gravitational buckle folds at the foot of the slope expressed as an anticlinal ridge and a synformal trough (south of Gavbast village) (39R 780250, 3031491). (B) Localized buckling slope failure showing convex-outward antiformal ridges and synformal troughs. This slope movement has largely buried a valley and has deflected its drainage (39R 788046, 3030846). (C) General view of the southern sector of Gavbast Dome, showing landslides Ls4 and Ls5 and an incipient pentagon-shaped rock slab failure with bulges and a wrinkle ridge at the downslope apex (incipient planar slide centered at 39R 785254, 3022932).

Table 1
Morphometric parameters of large landslides associated with Gavbast Dome and Kooh Bedoo Dome, where strata have been over-steepened and weakened by diapiric uplift. The dip of the strata and the deviation between the displacement direction and the dip direction is indicated, together with the geomorphic setting of the landslides. All the slope movements are controlled by bedding-controlled planar failures, except the rotational landslide LsW in Kooh Bedoo Dome.

Landslide	Length (km)	Width (km)	Area (km^2)	Volume (Mm^3)	Dip	Dip deviation	Setting
Gavbast Dome							
Ls1	1.1	0.73	0.4	8	19	0	dip slope
Ls2	1.9	0.53	0.64	13	19	70	flatiron edge
Ls3	2.1	0.66	1.1	23	18	65	dip slope
Ls4	5	1.6	4.4	190	18	30	flatiron edge
Ls5	2.5	2.4	3.5	140	18	0	dip slope
Ls6	1.3	0.38	0.4	12	17	28	flatiron edge
Ls7	3.9	1.15	2.9	59	19	0	dip slope
Ls8	4.7	4.1	9.4	260	19	0	dip slope
Kooh Bedoo Dome							
LsW	1.7	3	3.4	370	15		
LsE	2.4	1.2	2.4	150	15		dip slope

mapped landslides with areas larger than 0.4 km^2, the dip of the strata, the deviation between the displacement direction and the bedding dip (0–70°), and the geomorphic setting. Some landslides are located on dip slopes, whereas others (Ls2, Ls4, Ls6) have developed on the lateral slopes of large flatirons. The displacement direction of the latter shows significant deviation with respect to the dip of the underlying strata. The largest ones on the dome are landslides Ls4 and Ls5, with estimated volumes of 140 Mm^3 and 190 Mm^3, respectively (Fig. 9C). Landslide Ls5 is a relatively old and dissected slope movement, whereas landslide Ls4, which cross-cut the former, has fresh appearance and displays a secondary failure at the toe (Fig. 9C). Landslides Ls7 and Ls8, east of Lavarmistan village, occur in dip slopes underlain by marls and interbedded limestones of the Pabdeh Fm. and have estimated volumes of 59 Mm^3 and 260 Mm^3, respectively (Fig. 4). Landslide Ls8 is a long-runout rock avalanche that travelled across the piedmont and overriding by 50 m a ridge on the opposite flank of the valley.

Interestingly, the limestones of the Khami Group on the southern slope of the dome exhibit an incipient pentagon-shaped rock slab failure 2.6 km long and 2.9 km wide with the apex pointing downslope (Fig. 9C). Evidence of downslope displacement in this rock slab include (Fig. 9C): (1) an extensional trench 1.5 km long and 20 m wide in the head associated with an inward-dipping normal fault; (2) two lateral and diverging fault-controlled downhill-facing scarps; (3) internal bulges (buckling) in the lower part of the slab, expressed as bow-shaped downhill-facing scarps at the lower-east edge; (4) an uphill-facing scar on the lower-west edge generated by the upturning of the strata just below the rock slab; and (5) a conspicuous wrinkle ridge related to gravitational contraction at the downward-pointing apex of the slab.

The displaced portion of the dip slope displays a dense gully network abruptly interrupted and deflected at the downslope edge of the slope movement. Considering a modest hypothetical thickness for the rock slab of 50 m, with an area of 5.2 km^2, the slope collapse would involve a rock volume of ~260 Mm^3. This slope failure would be very likely followed by retrogressive planar slides affecting unconfined strata situated upslope and significantly weakened by dip-transverse normal faults with favorable orientation.

5. Kooh Bedoo Dome

5.1. Geology &geomorphology

The Kooh Bedoo structural dome is associated with a 125 km long, symmetric, WNW-ESE oriented anticline, designated as Nakh and Baviun anticline west and east of the salt structure, respectively. The Kooh Bedoo Dome occurs where this crank-shaped fold shows a sharp NE-SW bend with two inflections (Fig. 3). This deflection can be attributed to the control imposed the weak precursor salt stock on fold nucleation and propagation (Callot et al., 2007; Jahani et al., 2009; Jackson and Hudec, 2017). More specifically, the Kooh Bedoo salt dome is situated at the SW inflection of the bend, where the strike of the fold axis changes from NW-SE to NE-SW. Consequently, the buckle fold at the domal structure shows some asymmetry, with concave and convex (i.e., outward facing convexity) limbs in plan to the north and south, respectively (Fig. 10). Jahani et al. (2009), in two cross-sections traversing the Nakh-Baviun Anticline west and east of Kooh Bedoo Dome, respectively, depict wide wave-length detachment folds in a thick Phanerozoic cover, decoupled from the brittle basement along the Hormuz salt decollement at a depth of around 11–15 km (i.e., source layer of Kooh Bedoo stock). Berberian (1995), based on the distribution of the southernmost outcrops of the Asmari limestone, mapped his inferred Mountain Front Fault, a major blind, seismogenic, N-dipping reverse basement fault, along the southern flank of the Nakh-Baviun anticlinal ridge (Fig. 3). The topographic relief of the anticline in the vicinity of the dome reaches around 1550 m. Assuming that the fold started to create relief at ca. 2–3 Ma (base of the conglomeratic Bakhtyari Fm.; Homke et al., 2004; Ruh et al., 2014; Vergés et al., 2019), a minimum long-term uplift rate related to folding of $\geq$0.5–0.75 mm/yr can be estimated. See Mouthereau et al. (2007) and Gutiérrez et al. (2023) for additional details on the calculation of the minimum uplift rates.

The stratigraphy exposed in the mapped area is similar to that of the Gavbast Dome. The main differences include (Perry et al., 1965; NIOC, 2004b) (Fig. 10): (1) the youngest outcropping unit corresponds to limestones of the Early-Late Cretaceous Bangestan Group (Sarvak Fm. and Ilam Fm.), underlain by the non-exposed and mechanically weak marls and shales of the Kazhdumi Fm.; (2) the Gurpi (Late Cretaceous) and Pabdeh (Paleocene) formations are separated by a very thick unit of Jahrum dolomites and limestones (Eocene).

In the piedmonts on both sides of the anticlinal ridge, Quaternary alluvial fans unconformably overlying steeply dipping bedrock are offset by bedding-parallel flexural-slip faults, providing evidence for active folding and anticline growth (e.g., Walker et al., 2005, 2015; Gutiérrez et al., 2014, 2023; McCalpin et al., 2020) (Figs. 10 and 11). These surface-rupturing faults mainly occur associated with the Mishan and Agha Jari formations in the anticline limbs, and specially along the contact between both units with contrasting competence. The faults are expressed in the landscape as swarms of uphill-facing scarps that locally block drainages creating: (1) defeated streams and sediments traps in the downthrown block; and (2) perched beheaded valleys and wind gaps in the upthrown block. Local people take advantage of the antislope scarps for water ponding. Fig. 11 illustrates the main flexural-slip fault scarps identified in the southern piedmont, indicating the height of the scarps measured along transverse topographic profiles constructed with a hand-held rangefinder. To the SE of Noor Abad village there is a composite fault scarp associated with the Mishan-Agha Jari contact (ca. 60° dip) with a total height of 10.2 m (eastern sector of Fig. 11A). Here, the fault scarp is notched by a clear water wap associated with a highly sinuous abandoned channel in the upthrown block. The identified flexural-slip faults on the northern piedmont are restricted to a perched alluvial fan underlain by Mishan and Agha Jari formations (Fig. 10). In the southern piedmont, between Eslam Abad and Noor Abad, an alluvial fan and some drainages are offset by a NE-SW left-lateral strike-slip fault with down-to-the-west vertical component. This sinistral fault can be traced along the southern limb of the anticline offsetting bedrock units (Fig. 10). The fault in the alluvial fan is expressed as a NW-facing antislope scarp with measured heights of 1.8 m and 3 m at the corresponding points of two perpendicular profiles (276481E, 2993569N and 276749E, 2993844N, respectively).

The Kooh Bedoo salt structure, superimposed on the anticline and approximately 15 km long in the fold direction, can be identified on the basis of (Figs. 10 and 12): (1) the domal structure with centrifugal dips forming a complete pericline; (2) a culmination in the anticline hinge, clearly expressed by strata in the fold crest dipping longitudinally away from the dome (e.g., flatiron of Asmari in the NE flank); (3) a major transverse graben in the crestal and NW flank of the dome; and (4) a high concentration of large landslides developed on over-steepened slopes. The cross-section constructed partially along the axis of the fold and dome and the position of the Asmari Formation in the anticline crest in the vicinity of the dome indicate a local uplift related to diapiric doming of around 400 m. This value rises to ca. 1500 m on the opposite side of the dome, probably related to local undulations in the crest of the fold unrelated to diapirc doming (e.g., merging of propagating folds; Leturmy et al., 2010) (Fig. 12). The crestal zone of the anticline shows longitudinal normal faults and grabens with geomorphic expression attributable to outer arc extension. These normal faults are well exposed in the Jahrum carbonates exposed along the escarpment located on the NE sector of the dome (Fig. 13). The Kooh Bedoo domal structure shows a crater-like topography with an inner dome related to the erosional unroofing of the upwarped Asmari and Jahrum carbonate rocks and the rapid denudation of the Gurpi marls. This differential erosion process results in the exhumation of the top of the domed limestones of the Bangestan Group, which form most of the outcrops in the crater floor, interrupted by a large exposure of downthrown younger units (Gurpi and Jahrum) in the main graben.

5.2. Normal faults

The normal faults are identifiable in outcrops of Bangestan limestone, where they are clearly expressed as fault scarps. The mappable trace of the faults is locally interrupted in the easily erodible Gurpi marls that occur as local outliers and within the transverse graben. The main extensional structure is a fold-normal, NW-SE oriented graben restricted to the crest and NW flank of the dome, showing an abrupt SE termination. The graben width expands towards the edge of the dome from 1.2 km to 2 km, with a widening factor of 65%. The main NW-SE flanking faults, with mapped lengths of 2.5 and 3 km, are expressed as prominent scarps mainly attributable to differential erosion of the Gurpi marls in the downthrown block by deeply entrenched strike drainages. In this erosional context it is difficult to determine whether these faults are active or inactive (i.e., fault-line scarps). The cross-section constructed across the graben indicates a throw in its central sector of around 250 m. The SE termination of the graben in the crest of the dome is controlled by a series of NE-SW-striking en-echelon cross faults with right-stepping arrangement. Where these faults occur on Bangestan outcrops, they are expressed as well-defined linear scarps tens of meters high, suggesting current activity. In sections where the faults juxtapose Bangestan limestone against Gurpi marls in the downthrown block, differential erosion and artificial excavations have created scarps on exhumed fault planes, with dips of 50–55° and slickensides indicating dip-slip displacement (pitch 80–90°) (Fig. 13A and B; Fig. SM3 in

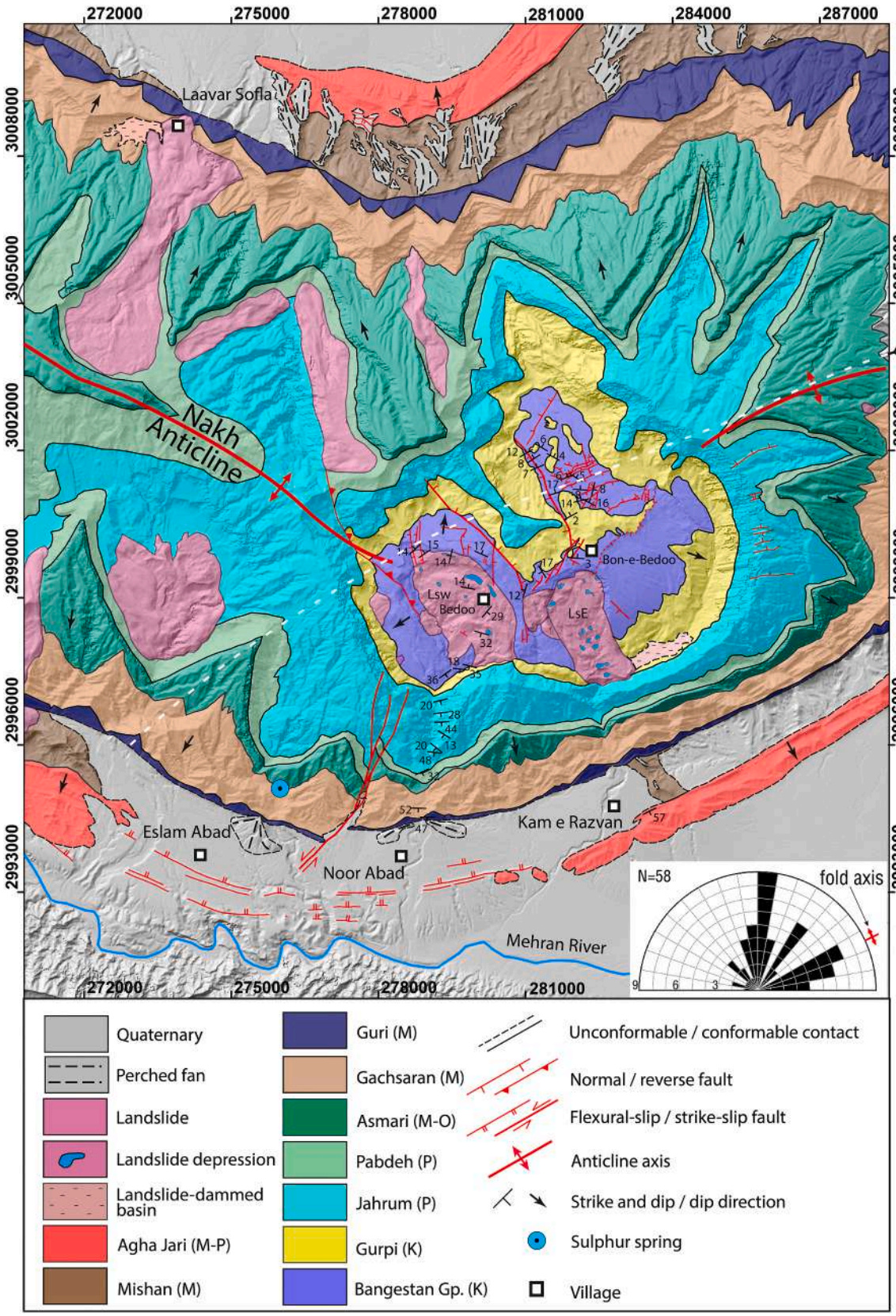

Fig. 10. Geological map of Kooh Bedoo Dome and associated structures related to a buried salt stock at a bend in the Nakh-Baviun Anticline. The dome shows a major transverse graben in the crest and NW flank. The map shows active flexural-slip faults that offset alluvial fans in the southern and northern piedmonts, as well as a Quaternary left-lateral strike slip in the southern limb. Note the extraordinary high concentration of large landslides. The trace of the cross-section shown in Fig. 12 is indicated with a white dashed line. Inset rose diagram indicates the frequency of the cartographic trend of normal faults mapped in the dome. P: Pliocene; M: Miocene: O: Oligocene; Pal: Paleogene; K: Cretaceous; J: Jurassic.

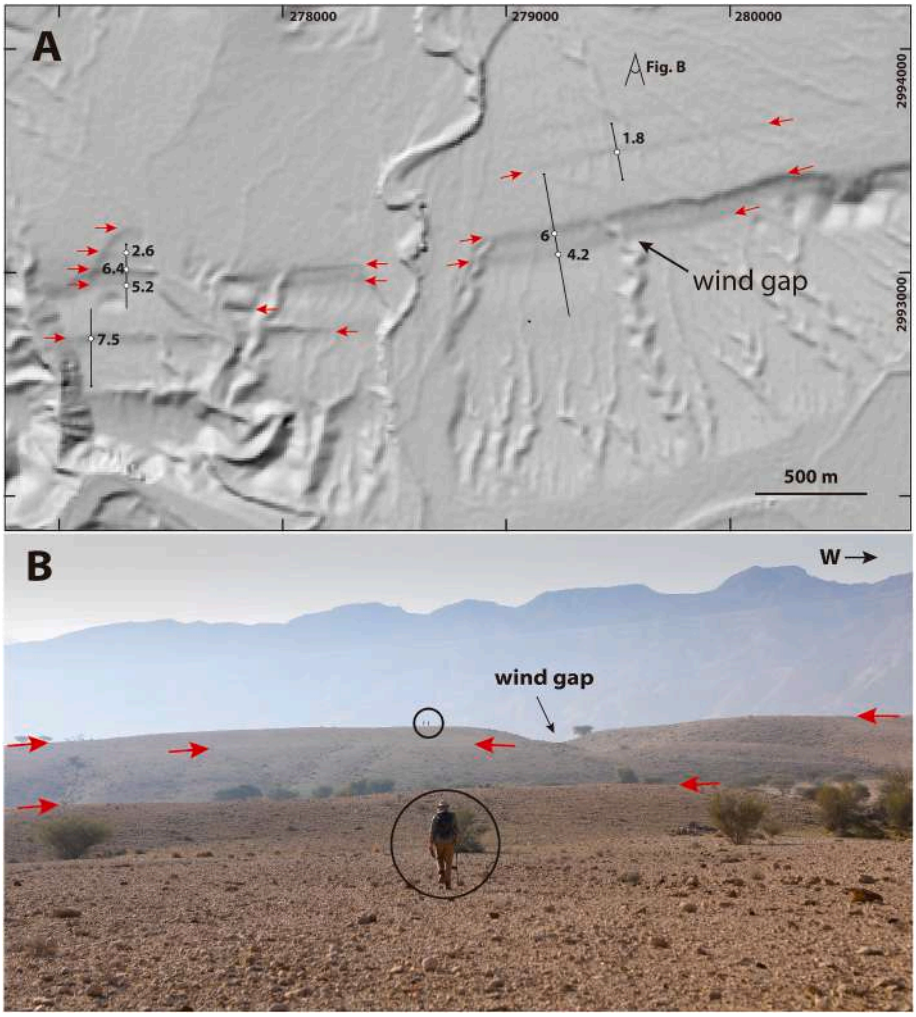

Fig. 11. Antislope flexural-slip fault scarps in alluvial fans at the southern piedmont of the Nakh-Baviun anticlinal ridge. (A) Shaded relief model showing the uphill-facing fault scarps (red arrows) and a perched and beheaded drainage (wind gap) on the upthrown side of a composite scarp 10.2 m high. Lines and points indicate the location of topographic profiles and scarp heights measured with a range-finder. (B) Frontal view of antislope scarps and wind gap. Circles indicates persons for scale. See location of image-shooting point in A (wind gap located at 40R 279432, 2993231).

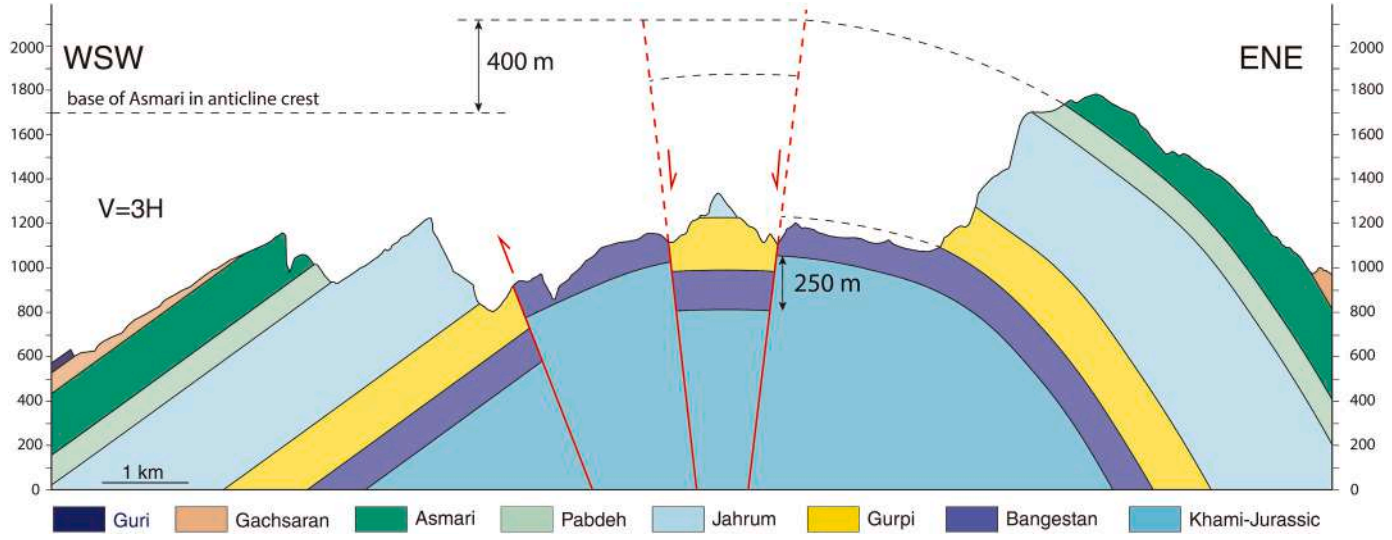

Fig. 12. Cross-section across Kooh Bedoo dome indicating approximate local uplift related to diapiric doming and throw of the crestal graben. Constructed with available thickness and strike and dip data from the exposed units and the TanDEM-X DEM. Thickness of not fully exposed units derived from NIOC (2004b). Trace of section indicated in Fig. 10. Vertical exaggeration x3.

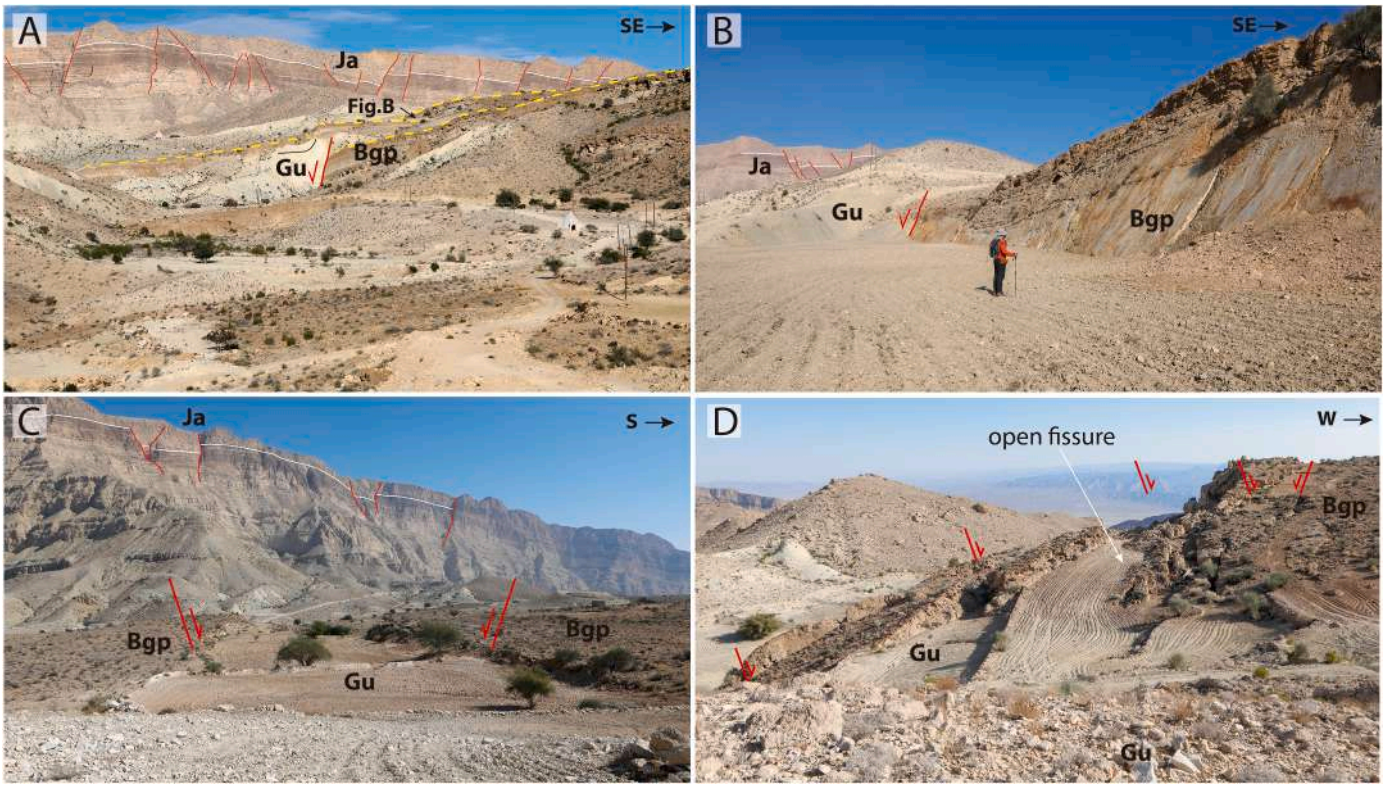

Fig. 13. Images of normal faults mapped in Kooh Bedoo diapiric dome. (A) General view of the SE termination of the main graben, with fault scarps on Bangestan limestone. Differential erosion of Gurpi marls in the downthrown block has exhumed fault planes with slickensides indicating dip-slip displacement (40R 281845, 2999949). In the background, fold-parallel faults in the hinge zone of the anticline attributable to outer-arc extension. (B) Exhumed fault plane generated by artificial excavation of Gurpi marls. See location in figure A (40R 282107, 3000069). (C) Fold-parallel ENE-WSW-oriented graben on the NE margin of the main graben. This depression is probably related to differential erosion of the soft Gurpi marls. Equivalent normal faults in the background ascribable to outer-arc extension (40R 282032, 3001587). (D) N-S oriented normal faults in the crest of the head scarp of the Bedoo landslide (beyond the ridge) with wide-open fissures likely related to local slope instability (40R 280270, 2999901).

Supplementary Material). Overall, the graben is expressed as a prominent NW-SE oriented ridge of Gurpi marls capped by resistant Jahrun dolomitic limestone, constituting an example of relief inversion.

The outcrops of Bangestan limestone located on the NW margin of the main graben display a series of fold-parallel, ENE-WSW-trending horst and grabens (Fig. 13C). These faults typically dip around 80° and have throws up to tens of meters. The grabens are often occupied by Gurpi marls and none of them is an enclosed basin. These extensional structures can be related to both outer-arc extension in the crest of the fold and doming. Equivalent faults are clearly observed in the adjacent cliffs on Jarum Formation and away from the dome, associated with the hinge zone of the fold. The horst and graben topography may be largely related to differential erosion of Gurpi marls and the faults may have limited activity. On the SW margin of the graben there is also a system of short N-S oriented normal faults with geomorphic expression that tend to form clusters. These faults show similar features to those located on the NE margin of the main graben. The scarps and graben depressions are likely related to differential erosion (i.e., fault-line scarps), and the limited evince of activity occurs associated with steep unstable scarps, suggesting some local shallow gravitational displacement (Fig. 13D). Interestingly, the short N-S trending faults are the most frequent, followed by the ENE-WSW fold-normal faults, whereas the NW-SE oriented faults with hectometer-scale throw are essentially restricted to the bounding faults of the main graben (see inset rose diagram in Fig. 10).

5.3. Landslides

The cartographic work performed reveals that the Kooh Bedoo dome and its vicinity shows an anomalously high concentration of large landslides (Fig. 10). The outcrops of Bangestan limestone with overall domal structure display two well-defined large landslides, here designated as landslide west (LsW) and landslide east (LsE). Landslide LsW represents the gravitational collapse of the over-steepened SW flank of the dome, scalloped by a large rotational slide (Fig. 14A). This slope movement is 3 km wide, 1.7 km long and covers an area of 3.4 km^2. The curved deep-seated sliding surface is likely controlled by shales of the Kazhdumi Fm. underlying the limestones of the Bangestan Group. A volume of 370 Mm^3 has been roughly calculated considering an ellipsoidal geometry for the failure plane and interpreting its position through the construction of longitudinal sections. The crescent-shaped head scarp of the landslide, around 100 m high, displays abundant evidence of recent-active displacement pointing to its retrogressive propagation. These include large coherent detached and down-dropped blocks (NW edge), and fresh-looking grabens and fissures. At the foot of the headscarp there is a conspicuous elongated depression attributable to a keystone graben bounded by downhill- and uphill-facing scarps (Fig. 14B). In the upper part of the landslide, where the Bedoo village is sited, backtilted strata dip into the slope. Below, the landslide deposits have been largely transformed into a mega-breccia, locally interrupted by large coherent rock masses with anomalous dips. In the southern edge, the landslide toe has over-ridden the opposite slope on Gurpi marls.

The landslide LsE is located next to the SE termination of the main NW-SE-trending graben, resembling its projection (Figs. 10 and 14C). The lateral edges of this elongated landslide are probably controlled by concealed NW-SE normal faults, but with limited vertical offset as indicates the lack of downthrown Gurpi marls. This fresh-looking landslide has a headscarp of up to 150 m high. The landslide deposits reach

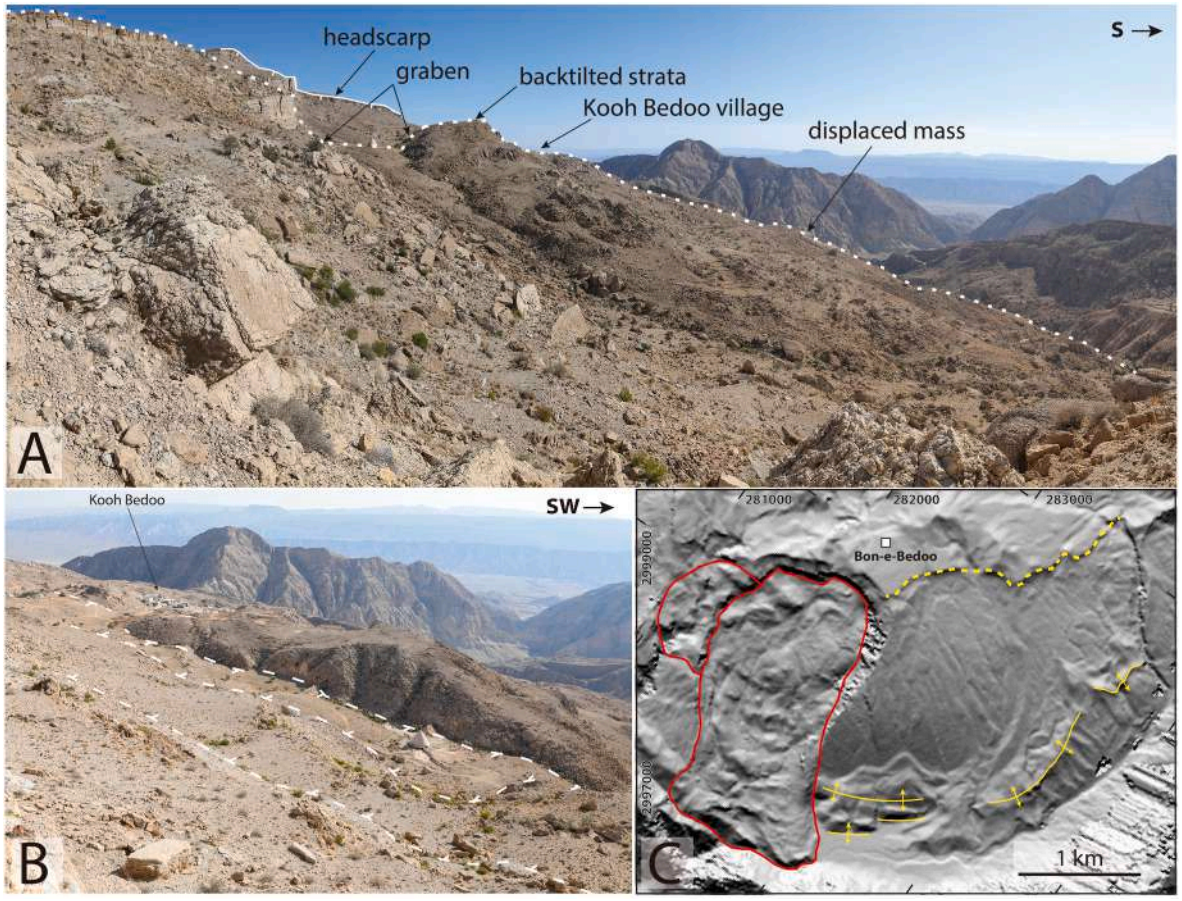

Fig. 14. Slope movements in Kooh Bedoo Dome. (A) Lateral view of landslide LsW from its NE edge. Note graben and backtilting in the upper part of the displaced mass. (B) Keystone graben in the upper part of landslide LsW bounded by downhill- and uphill-facing scarps. Kooh Bedoo village in the downslope margin of the graben (40R 279656, 2999604). (C) Shaded relief model of the SE sector of the dome showing landslide LsW (red lines) and an incipient slope failure (yellow lines). Landslide LsW is a rock slide-flow that has buried a valley at its foot creating a landslide-dammed basin. The incipient gravitational slope deformation is expressed by a sinuous downhill-facing scarp in the upper part and local buckle folding in the lower section of the slope.

2.4 km and 1.2 km in length and width, respectively, and cover an area of 2.4 km^2. This slope movement is interpreted as a planar rock slide-flow that has experienced significant disintegration. A volume of 150 Mm^3 has been roughly estimated considering a bedding-controlled sliding surface (Kazhdumi shales?) inferred from longitudinal sections. The slope movement has a hummocky topography riddled by enclosed depressions. Its toe has buried the stream that flows along the periphery of the dome, eventually creating a landslide-dammed basin currently with open drainage.

The convex dip slopes of the dome NE of landslide LsE display evidence of an incipient landslide (Figs. 10 and 14C). This embryonic slope failure displays along its upper edge, SE of Bon-e-Bedoo village, a sinuous downhill-facing scarp, roughly coinciding with the crest-to-limb transition of the structural dome. In the lower part of the slopes strata of Bangestan and Gurpi display local buckle folds attributable to bedding-controlled sliding and local contraction by detachment folding in the pinned lower section. The sector showing this gravitational slope deformation cover an area of 5.3 km^2. This slope movement would involve a volume of around 250 Mm^3 in case it would affect a stratigraphic package around 50 m thick. On the northern limb of the dome and anticline there are four large slide-flows sourced from steep slopes underlain by Pabdeh marls with interbedded limestone. The largest one, 5.4 km long and 6.7 km^2 in area, has created a landslide-dammed basin used for cultivation by the inhabitants of Laavar Sofla village, sited on the landslide toe (Fig. 10).

6. Discussion

6.1. Uplift by buckle folding and active diapirism

Stratigraphic and structural evidence indicates that most Homuz salt diapirs in the Fars Arc of the Zagros Belt already existed before the onset of the Cenozoic collision. These precursor diapirs experienced long-lasting pre-orogenic growth coevally to the sedimentation of a thick and essentially flat-lying overburden (i.e., downbuilding) (Harrison, 1930; Kent, 1979; Jahani et al., 2007, 2009; Snidero et al., 2019). Some diapirs, like the ones analyzed in this work, became inactive during a protracted period of time (e.g., late Paleozoic-Miocene) and were buried at least by the thick Mesozoic succession exposed in the current doming and erosional stage. During the ongoing Cenozoic collision, the southward-migrating regional shortening has produced wide-wavelength detachment folds in a Phanerozoic cover around 11–15 km thick overlying the Neoproterozoic-Cambrian Hormuz salt (Jahani et al., 2009). The weak salt plugs functioned as strain enhancers and localizers, controlling the nucleation of anticlines and determining deflections in their lateral propagation path (Letouzey and Sherkati, 2004; Callot et al., 2007; Jahani et al., 2007, 2009). Folding is accompanied by the creation of concordant relief (i.e., growing anticlinal ridges and synclinal valleys) and the contraction of the salt plugs inducing their rejuvenation by displacement loading. Active diapirism related to the rise of the squeezed salt tends to inflate the roof of buried salt stocks, producing uplifting domal structures along the axes of the growing anticlines. These morpho-structures affected by concomitant

buckle folding (i.e., fold-normal layer-parallel compression) and doming are sites of: (1) enhanced structural relief and topography; (2) high spatial frequency of normal faults and fractures, leading to significant rock mass weakening; (3) over-steepening of strata and slopes by upward and outward rotation; (4) high density of large landslides; and (5) future locations for salt extrusions (passive diapirism). The time-transgressive basal unconformity of the Bakhtyari conglomerates, dated by magnetostratigraphy in the studied region close to the Deformation Front at ca. 3-2 Ma (Homke et al., 2004; Ruh et al., 2014; Vergés et al., 2019), most probably records the onset of vigorous morphogenetic folding (Mouthereau et al., 2007; Gutiérrez et al., 2023) and intense contractional loading in the buried salt plugs. The documented widespread flexural-slip faults that rupture Quaternary alluvial fans in the piedmonts of the anticlinal ridges provide evidence of ongoing active folding in the analyzed anticlines (Fig. 3B and 11). The anticlinal ridges where the Gavbast and the Kooh Bedoo domes occur show a local relief of 1200–1550 m, suggesting long-term uplift rates related to folding of ≥0.4–0.7 mm/yr. Similar uplift rates of 0.3–0.6 mm/yr were estimated for folds in the central-western sector of the Fars Arc by Mouthereau et al. (2007). The structural relief created by local active diapirism in Gavbast and Kooh Bedoo domes, given by the upward bulging of strata in the anticline crests, has been estimated on the basis of cross-sections at 1300 and 400 m, respectively (Figs. 5 and 12). Long-term uplift rates related to doming of 0.1–0.4 mm/yr can be estimated assuming that most of the arching in the diapir roof has occurred over the last 3 Ma. Actual rates could be lower due to possible pre-orogenic uplift of the diapir roof (Jahani et al., 2009) and the initiation of the diapir rejuventation before the vigorous folding phase.

6.2. Normal faults

The elliptical Gavbast Dome displays three main sets of normal faults with heterogeneous distribution (Figs. 4 and 6). (1) transverse fold-normal faults; (2) longitudinal fold-parallel faults; and (3) multidirectional oblique normal faults perpendicular to dip direction related to radial extension. The complex distribution of the different fault sets can be related to a number of factors, including: (1) the variable along-strike geometry of the folding structure, with a west-plunging synclinal pericline and an antiform on the western and eastern edges of the dome, respectively; (2) the elliptical shape of the dome parallel to fold axis; and (3) the superposition of far-field compressional forces and local multidirectional extension induced by active diapirism. The longitudinal faults in the SE flank associated with the anticlinal structure can be attributed to outer-arc extension related to buckle folding enhanced by local doming, plus the elliptical shape of the dome. Physical models reveal that normal faults developed in elliptical domes trend dominantly parallel to the dome axis (Withjack and Scheiner, 1982; Sims et al., 2013). The fold-normal grabens on the NW sector suggest greater transverse extension in this portion of the dome, and that far-field compressional forces have suppressed the local fold-normal extensional forces related to doming, as illustrated by physical models (Withjack and Scheiner, 1982; Sims et al., 2013). Moreover, in this sector bending-moment normal faulting related to outer-arc extension can be inhibited by the adjacent synclinal folding. The polygonal system of horst and grabens in the crestal zone, with multiple minor enclosed depressions, seems to be rather peculiar, since most natural and experimental examples display a single circular or polygonal crestal graben (McDowell, 1951; Parker and McDowell, 1955; Withjack and Scheiner, 1982; Schmidtz and Flizeder, 1993; Davison et al., 2000; Stewart, 2006). This difference is probably related to the broad crestal zone of Gavbast Dome and the presence of anisotropies (i.e., fractures) that do not occur in unconsolidated sediments and are not accounted for in experimental physical models.

The Kooh Bedoo Dome, located at an inflection point of a sinuous anticline, displays a major transverse graben restricted to the crest and NW flank of the dome, with an abrupt SE termination controlled by en echelon faults (Figs. 10 and 12). The fold-normal orientation of this main graben suggests that regional compression suppresses the doming-related extensional forces in the shortening direction, resulting in a local stress field dominated by fold-parallel extension (Withjack and Scheiner, 1982) (Fig. 1). The fold-normal asymmetry of the structure across dome is probably related to the location of the salt plug at an inflection point of the anticline, with concave geometry in plan on the "with-graben" limb and a convex shape on the "without-graben" limb. The NE margin of the graben shows a system of fold-parallel horsts and grabens with meter-to decameter-scale throws compatible with both outer-arc extension in the hinge zone of the anticline and doming. The geomorphic expression of these structures may be related to the combined effect of differential erosion of soft Gurpi marls in the downthrown blocks and fault activity. Experimental physical models reproducing the structural configuration of the domes might provide further insight into the fault pattern observed at Gavbast and Kooh Bedoo (e.g., Sims et al., 2013).

The mapped faults are most probably active, since they are consistent with the current stresses related to: (1) regional shortening; (2) active diapirism activated by contractional loading, (3) and outer-arc extension induced by both buckle folding and doming. Nonetheless, several lines of evidence suggest that slip rates are relatively slow, including: (1) lack of fresh scarps; (2) limited disruption of the drainage network; and (2) enclosed basins restricted to the relatively flat crestal zone of Gavbast, where fluvial dissection has limited impact. Trenching across faults and DInSAR data would allow to constrain the activity and kinematics of these supra-salt faults, as well as the flexural-slip faults that rupture Quaternary deposits on the anticline limbs.

6.3. Landslides

The analyzed domes display an extraordinarily high density of large landslides, often with volumes greater than 100 Mm^3, revealing that slope movements can play an instrumental role in the unroofing of rising salt plugs and salt emergence (see cartographic inventory of landslides in the Zagros by Ghazipour and Simpson, 2017). In the studied examples they mostly correspond to planar failures controlled by mechanically weak argillaceous units underlying thick resistant limestone packages. Landslides on the southern dip slopes of Gavbast Dome, including a 5.2 km^2 incipient rock slab failure, cover an aggregate area of 13.6 km^2. At Kooh Bedoo Dome, the landslides and an embryonic planar slope failure cover a total area of 11.1 km^2, representing 40% of the domal relief.

Both domes display peculiar gravitational slope deformation features, characterized by the downslope sliding of coherent stratigraphic packages along weak units (e.g., Kazhdumi Fm.) producing detachment anticlinal ridges and synclinal troughs in the lower part of the pinned slopes (Figs. 9 and 14). Molinaro et al. (2005) documented similar "parasitic" folds affecting Guri limestone detached along the underling Razak marls (chronostratigraphically equivalent to Gachsaran evaporites) in the limbs of growing anticlines at the eastern sector of the Fars Arc. They attributed these disharmonic structures to gravitational sliding induced by the amplification and steepening of the growing anticlinal ridges. Equivalent bedding-controlled gravitational gliding associated with diapirs has been also reported offshore with seismic data, where they are designated as delamination extensional structures (Owen and Taylor, 1983; Coward and Stewart, 1995; Nilsen et al., 1995; Jackson and Hudec, 2017). This slow gravitational slope deformation process may precede the development of well-defined landslides and have significant implications from the hazard perspective, inasmuch as they may eventually evolve into catastrophic long-runout rock avalanches. Gravitational buckle folding has been reported in slopes that have sourced major rock avalanches. It has been observed on Pabdeh marls and limestones in the unloaded scar of the gigantic Seymareh rock avalanche (44,000 Mm^3, 220 km^2), considered the largest subaerial rock slope failure worldwide (Lurestan Arc, Zagros Mountains; Delchiaro et al., 2019). It has been proposed that progressive buckle folding in steeply dipping, well-bedded successions and the associated rock mass

weakening may precede catastrophic slope failures. Some examples include the 25 Mm^3 2009 Shiaolin rock slide-avalanche, Taiwan, that caused 400 casualties (Tsou et al., 2011), or the 18 Mm^3, 2017 Xinmo rock avalanche, China, resulting in 102 casualties (Zhao et al., 2018).

The main predisposing factors for landslide development in the analyzed domes are the presence of concordant dip slopes on stratigraphic successions comprising thick resistant limestone packages underlain by weak marl and shale units where the planar or rotational sliding surfaces develop (Ghazipour and Simpson, 2017). The key preparatory factors, that refer to dynamic changes shifting a slope to a marginally stable state, include: (1) fracturing and faulting that weaken the rock mass and create favorable release and breakout planes for the detachment of rock slabs; (2) the progressive over-steepening of the dip of the strata and the gradient of the slopes. Both processes are mainly related to active diapirism, involving multidirectional extension in the roof of the salt stocks and upward and outward rotation in the flanking slopes. Potential triggers for the initiation of the slope failures or the transition of creeping slope deformation into a rapid movement include seismic shaking, slope undermining and heavy rainstorms. Large earthquakes can play a very important role as landslide triggers in the Zagros Mountains, which is one of the most seismically active regions in the world (Talebian and Jackson, 2004; Karasözen et al., 2019; Gutiérrez et al., 2023).

6.4. Erosional unroofing and salt breakout

Salt rise in a buried salt plug causes roof uplift, which tends to be counterbalanced by erosional unroofing. These processes involve the progressive upward displacement of the top of the salt and the thinning of the diapir's roof. Eventually, the salt may breakout at sites where the overburden has been sufficiently thinned and weakened by erosion and deformation (e.g., normal faulting, gravitational slope deformation).

In the Fars Arc of the Zagros, where the overburden is characterized by alternating packages of resistant carbonate formations (e.g., Khami and Bangestan groups) and easily erodible and mechanically weak shales and marls (e.g., Kazhdumi, Gurpi, Pabdeh formations), two main erosional styles with contrasting spatial-temporal patterns operate. Water erosion in carbonate outcrops with high infiltration capacity (low runoff coefficient) and in a semiarid climate proceeds at very slow rates. However, as illustrated by the Gavbast and Kooh Bedoo domes, limestone caprocks in over-steepened slopes weakened by faulting can be locally and rapidly eroded by massive landslides, mostly controlled by planar failures developed along underlying or interbedded weak units. Erosional unroofing dominated by landsliding is also illustrated by the Narou Dome south of Shiraz (see location in Fig. 3A). Once the resistant caprock is removed and the underlying clay-rich formation is exposed, erosion is mainly achieved by fluvial dissection. Domal reliefs underlain by easily erodible sediments typically display a radial drainage network, nicely illustrated by Kharman Dome (the Farsi word Kharman means dome; Fig. 15A) and Sour Dome east and south of Shiraz, respectively (see location in Fig. 3A).

In domes disrupted by major grabens, the drainage net and fluvial entrenchment may be controlled by the graben depressions, which tend to show a fold-normal orientation. Transverse incising drainages guided by grabens occur in the NW sector of Gavbast Dome and in Darang Dome south of the Kuh-e-Namak salt extrusion (Fig. 15B). The latter is a structural dome breached by a major graben with significant down-to-the-NE offset across the structure. In the Fars Arc, episodic landsliding and gradual fluvial erosion, favored and/or guided by normal faulting, are probably the main erosional processes involved in the breakout of the salt and the onset of passive diapirism. Anguru salt extrusion in eastern Fars provides an example of a dome breached by a major graben formerly dissected by fluvial erosion (Fig. 15C). Probably, the breakout of a number of the salt extrusions was initiated by landslides, but their deposits are likely overridden and concealed by salt sheets (i.e., namakiers). An example is provided by Dadenjan salt extrusion

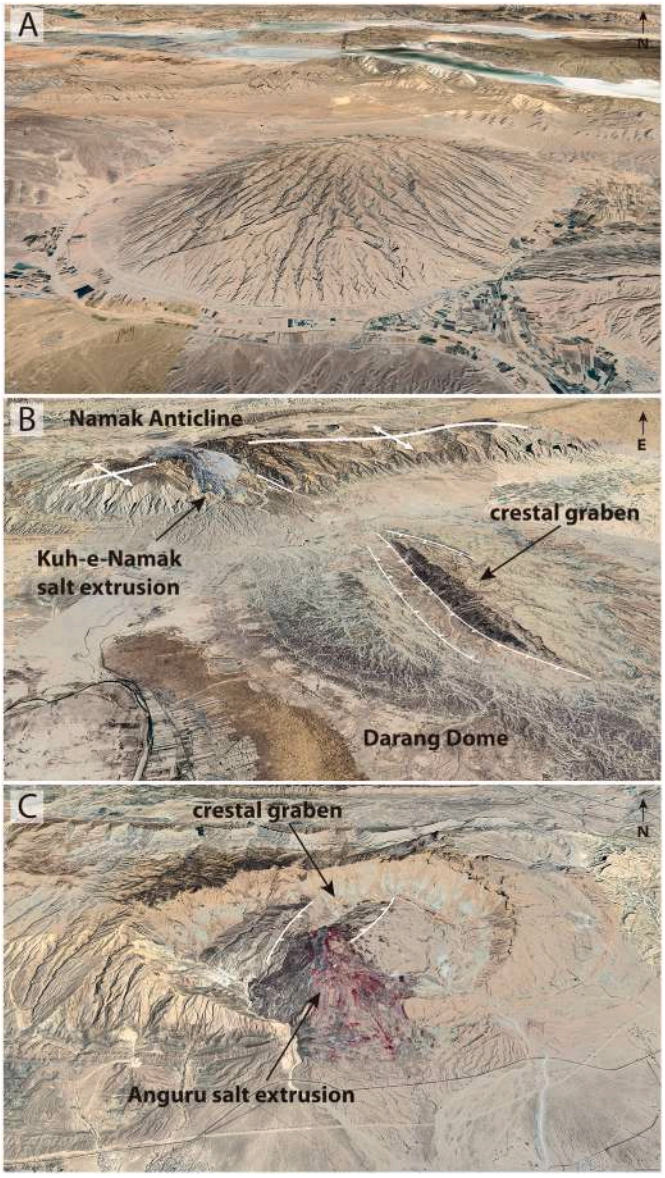

Fig. 15. Images captured from Google Earth (2023 CNES/Airbus) illustrating deformation and erosion processes involved in the unroofing of buried salt stocks in Zagros Mountains. See location of diapiric structures in Fig. 3A. (A) The 18 km long Kharman Dome, with a local relief of around 1600 m, dissected by a radial drainage carved into the carbonate Asmari and Jahrum formation, with a high proportion of marls. (B) Darang Dome south of Kuh-e-Namak salt extrusion associated with a right-lateral fault with limited offset. Darang Dome is breached by a crestal graben perpendicular to the NW-SE folding trend and drained by axial streams. The graben shows significant down-to-the-NW offset across the structure, being Khami Group (Cretaceous) and Agha Jari Fm. (Mio-Pliocene) the oldest rocks exposed on the SE and NW margin, respectively. (C) Anguru salt extrusion and south flowing namakier emerging from the floor of a fold-normal graben breaching a dome on limestones of the Khami Group. The graben displays axial drainage still preserved on the northern portion of the structure. Note dome nested in a crater similar to Kooh Bedoo dome.

associated Karezun strike-slip fault (see location in Fig. 3A) and with extensive landslide deposits abutting its southern flank. Physical models suggest that salt in squeezed stocks initially extrudes at sites where the overburden has been weakened and thinned by normal faulting (Dooley et al., 2015). These models do not reproduce long-term erosional processes such as creep gravitational deformation that evolve into large landslides, or gradual fluvial erosion, which according to geological evidence seem to also play an important role.

7. Conclusions

The cartographic analysis of two morpho-structural domes related to buried salt stocks associated with growing anticlines in the Zagros Mountains illustrates that domal structures can display complex normal fault patterns resulting from the interplay of regional and local stress fields, including far-field compression, doming-related multidirectional extension, and outer-arc extension in the hinge zone of the anticlines. The most significant extensional structures in this context, which correspond to fold-normal grabens with hectometer-scale throw, can be attributed, in agreement with experimental models, to the suppression of the doming-related extension in the direction of regional compression, resulting local fold-parallel extension. The superposition of fold-normal, fold-parallel and multidirectional dip-nomal faults in the crestal sector of the domes may produce polygonal systems of horsts and enclosed grabens bounded by dilated, high-permeability normal faults. The substantial spatial heterogeneity of the fault patterns can be ascribed to local factors such as: (1) complexities in the folding structure (e.g., bends, periclines); (2) plan shape of the domes (circular versus elliptical); (3) local transverse extension in the hinge zone of anticlines; and (4) overburden anisotropies.

Uplifting domes are particularly prone to the development of landslides, which may cover as much as 40% of the surface area. Overburdens consisting of thick resistant limestone packages and mechanically weak argillaceous units can be affected by large gravitational slope deformations expressed as buckle folds in the lower part of the slopes. These slow-moving incipient planar landslides with failure planes controlled by the weak argillaceous units may evolve into catastrophic landslides with volumes of the order of 10^8 m^3. The development of large slope failures is favored by rock mass weakening related to faulting and slope and dip over-steepening, both related to doming.

Episodic landsliding and more gradual fluvial incision often controlled by grabens, are the main erosional styles involved in the unroofing of the buried salt plugs in the study area, eventually leading to salt emergence and the development of namakiers (i.e, subaerial salt sheets). Landsliding dominates on dip slopes underlain by resistant limestone units, whereas fluvial incision is the prevailing erosional process in exposures of clay-rich formations. The analyzed domes provide factual data on the role played by factors and processes difficult to incorporate in experimental models, such as overburden anisotropies or long-term erosional processes including creeping-catastrophic slope movements and fluvial incision.

Declaration of competing interest

The authors declare that they have no known competing financial interests or personal relationships that could have appeared to influence the work reported in this paper.

Data availability

Data will be made available on request.

Acknowledgements

The work by FG was supported by a Salvador de Madariaga grant (PR19/00028) and projects (CGL2017-85045-P, DIAPERNO: PID2021-123189NB-I00) of the Spanish Government (Ministerio de Ciencia e Innovación). The TanDEM-X digital elevation models were provided by the German Aerospace Center (DLR; grant DEM_GEOL288). Authors are very grateful to Soumyajit Mukherjee (Associate Editor) and two anonymous reviewers for their insightful comments.

Appendix A. Supplementary data

Supplementary data to this article can be found online at https://doi.org/10.1016/j.marpetgeo.2023.106376.

References

Almalki, K.A., Ailleres, L., Betts, P.G., Bantan, R.A., 2015. Evidence for and relationship between recent distributed extension and halokinesis in the Farasan Islands, southern Red Sea, Saudi Arabia. Arabian J. Geosci. 8, 8753–8766.
Alsop, G.I., 1996. Physical modelling of fold and fracture geometries associated with salt diapirism. In: Alsop, G.I., Blundell, D.J., Davison, I. (Eds.), Salt Tectonics, vol. 100. Geological Society Special Publication, pp. 227–241.
Authemayou, C., Bellier, O., Chardon, D., Benedetti, L., Malekzade, Z., Claude, C., Angeletti, B., Shabanian, E., Abbassi, M.R., 2009. Quaternary slip-rates of the Kazerun and the Main Recent Faults: active strike-slip partitioning in the Zagros fold-and-thrust belt. Geophys. J. Int. 178, 524–540.
Berberian, M., 1995. Master "blind" thrust faults hidden under the Zagros folds: active basement tectonics and surface morphotectonics. Tectonophysics 241, 193–224.
Berberian, M., 2014. Earthquakes and Coseismic Surface Faulting on the Iranian Plateau. Elsevier, Amsterdam.
Bordenave, M.L., Hegre, J.A., 2010. Current distribution of oil and gas fields in the Zagros Fold Belt of Iran and contiguous offshore as the result of the petroleum systems. In: Leturmy, P., Robin, C. (Eds.), Tectonic and Stratigraphic Evolution of the Zagros and Makran during the Mesozoic-Cenozoic, vol. 330. Geological Society, London, Special Publication, pp. 291–353.
Callot, J.P., Jahani, S., Letouzey, J., 2007. The role of pre-existing diapirs in fold and thrust belt development. In: Lacombe, O., Roure, F., Lavé, J., Vergés, J. (Eds.), Thrust Belts and Foreland Basins. Springer, Berlin, pp. 1–17.
Clausen, O.R., Egholm, D.L., Andresen, K.J., Wesenberg, R., 2014. Fault patterns within sediment layers overlying rising salt structures: a numerical modelling approach. J. Struct. Geol. 58, 69–78.
Coward, M., Stewart, S., 1995. Salt-influenced structures in the Mesozoic-Tertiary cover of the southern North Sea, UK. In: Jackson, M.P.A., Roberts, D.G., Snelson, S. (Eds.), Salt Tectonics: A Global Perspective, vol. 65. American Association of Petroleum Geologists Memoir, Tulsa, OK, pp. 229–250.
Cloos, E., 1955. Experimental analysis of fracture patterns. Geol. Soc. Am. Bull. 66, 241–256.
Cloos, E., 1968. Experimental analysis of Gulf Coast fracture patterns. AAPG (Am. Assoc. Pet. Geol.) Bull. 52, 420–444.
Davison, I., Bosence, D., Alsop, G.I., Al-Aawah, H., 1996. Deformation and sedimentation around active Miocene salt diapirs on the Tihama Plain, northwest Yemen. In: Alsop, G.I., Blundell, D.J., Davidson, I. (Eds.), Salt Tectonics, vol. 100. Geological Society, London, Special Publication, pp. 23–39.
Davison, I., Alsop, I., Birch, P., Elders, C., Evans, N., Nicholson, H., Rorison, P., Wade, D., Woodward, J., Young, M., 2000. Geometry and late-stage structural evolution of Central Graben salt diapirs, North Sea. Mar. Petrol. Geol. 17, 499–522.
Delchiaro, M., Della Seta, M., Martino, S., Dehbozorgi, M., Nozaem, R., 2019. Reconstruction of river valley evolution before and after the emplacement of the giant Seymareh rock avalanche (Zagros Mts., Iran). Earth Surf. Dyn. 7, 929–947.
De Waele, J., Gutiérrez, F., 2022. Karst Hydrogeology, Geomorphology and Caves. Wiley, Chichester.
Dooley, T.P., Jackson, M.P.A., Hudec, M.R., 2009. Inflation and deflation of deeply buried salt stocks during lateral shortening. J. Struct. Geol. 31, 582–600.
Dooley, T.P., Jackson, M.P.A., Hudec, M.R., 2015. Breakout of squeezed stocks: dispersal of roof fragments, source of extrusive salt and interaction with regional thrust faults. Basin Res. 27, 3–25.
Edgell, H.S., 1996. Salt tectonism in the Persian Gulf basin. In: Aslop, G.I., Blundell, D.J., Davison, I. (Eds.), Salt Tectonics, vol. 100. Geological Society London Special Publication, pp. 129–151.
Gaullier, V., Vendeville, B.C., 2005. Salt tectonics driven by sediment progradation: Part II Radial spreading of sedimentary lobes prograding above salt. AAPG (Am. Assoc. Pet. Geol.) Bull. 89, 1081–1089.
Ghazipour, N., Simpson, G., 2017. Size distribution and controls of landslides in the Zagros mountain belt (Iran). Tectonic evolution, collision, and seismicity of Southwest Asia. In: Sorkhabi, E. (Ed.), Honor of Manuel Berberian's Forty-Five Years of Research Contributions, vol. 525. The Geological Society of America Special Paper, pp. 1–21. Tectonic Evolution, Collision and Seismicity of Southwest Asia.
Gutiérrez, F., Carbonel, D., Kirkham, R.M., Guerrero, J., Lucha, P., Matthews, V., 2014. Can flexural-slip faults related to evaporite dissolution generate hazardous earthquakes? The case of the Grand Hogback monocline of west-central Colorado. GSA Bulletin 126, 1481–1494.
Gutiérrez, F., Deirnik, H., Zarei, M., Medialdea, A., 2023. Geology, geomorphology and geochronology of the coseismic? Emad Deh rock avalanche associated with a growing anticline and a rising salt diapir, Zagros Mountains, Iran. Geomorphology 421, 108527.
Harrison, J.V., 1930. The geology of some salt-plugs in Laristan, southern Persia. Q. J. Geol. Soc. 86, 463–522.
Hessami, K., Koyi, H.A., Talbot, C.J., Tabasi, H., Shabanian, E., 2001. Progressive unconformities within an evolving foreland fold–thrust belt, Zagros Mountains. J. Geol. Soc. 158, 969–981.
Homke, S., Vergés, J., Garcés, M., Emami, H., Karpuz, R., 2004. Magnetostratigraphy of miocene-pliocene Zagros foreland deposits in the front of the push-e kush arc (lurestan province, Iran). Earth Planet Sci. Lett. 225, 397–410.
Jackson, M.P.A., Hudec, M.R., 2017. Salt Tectonics. Principles and Practice. Cambridge University Press, Cambridge.
Jahani, S., Callot, J.P., Frizon de Lamotte, D., Letouzey, J., Leturmy, P., 2007. The salt diapirs of the eastern Fars Province (Zagros, Iran): a brief outline of their past and

present. In: Lacombe, O., Roure, F., Lavé, J., Vegés, J. (Eds.), Thrust Belts and Foreland Basins. Springer, Berlin, pp. 289–308.
Jahani, S., Callot, J.P., Letouzey, J., Frizon de Lamotte, D., 2009. The eastern termination of the Zagros Fold-and-Thrust Belt, Iran: structures, evolution, and relationships between salt plugs, folding, and faulting. Tectonics 28, TC6004.
Jahani, S., Hassanpour, J., Mohammadi-Firouz, S., Letouzey, J., de Lamotte, D.F., Alavi, S.A., Soleimany, B., 2017. Salt tectonics and tear faulting in the central part of the Zagros Fold-Thrust Belt, Iran. Mar. Petrol. Geol. 86, 426–446.
Karasözen, E., Nissen, E., Bergman, E.A., Ghods, A., 2019. Seismotectonics of the Zagros (Iran) from orogen-wide, calibrated earthquake relocations. J. Geophys. Res. Solid Earth 124, 9109–9129.
Kent, P.E., 1979. The emergent Hormuz salt plugs of southern Iran. J. Petrol. Geol. 2, 117–144.
Letouzey, J., Sherkati, S., 2004. Salt movement, tectonic events, and structural style in the central Zagros Fold and thrust belt (Iran). In: 24th Annual GCSSEPM Foundation. Bob F. Perkins Research Conference: Salt-Sediment Interactions and Hydrocarbon Prospectivity: Concepts, Applications, and Case Studies for the 21st Century, Gulf Coast Section. Society for Sedimentary Geology, Houston, Texas.
Leturmy, P., Molinaro, M., de Lamotte, D.F., 2010. Structure, timing and morphological signature of hidden reverse basement faults in the Fars Arc of the Zagros (Iran). In: Leturmy, P., Robin, C. (Eds.), Tectonic and Stratigraphic Evolution of Zagros and Makran during the Mesozoic-Cenozoic. Geological Society, vol. 330. Special Publications, London, pp. 121–138.
Link, T.A., 1930. Experiments relating to salt-dome structures. AAPG (Am. Assoc. Pet. Geol.) Bull. 14, 483–508.
McCalpin, J.P., Gutierrez, F., Bruhn, R.L., Guerrero, J., Pavlis, T.L., Lucha, P., 2020. Tectonic geomorphology and late Quaternary deformation on the Ragged Mountain fault, Yakutat microplate, south coastal Alaska. Geomorphology 351, 106875.
McDowell, A.N., 1951. The Origin of the Structural Depression above Gulf Coast Salt Domes with Particular Reference to Clay Creek Dome, Washigton County, Texas. M. Sc. Thesis. Texas A&M University, p. 26.
Molinaro, M., Leturmy, P., Guezou, J.C., Frizon de Lamotte, D., Eshraghi, S.A., 2005. The structure and kinematics of the southeastern Zagros fold-thrust belt, Iran: from thin-skinned to thick-skinned tectonics. Tectonics 24, TC3007.
Motiei, H., 1993. Stratigraphy of Zagros. Geological Survey of Iran, Tehran.
Mouthereau, F., Tensi, J., Bellahsen, N., Lacombe, O., De Boisgrollier, T., Kargar, S., 2007. Tertiary sequence of deformation in a thin-skinned/thick-skinned collision belt: the Zagros Folded Belt (Fars, Iran). Tectonics 26, TC5006.
Mukherjee, S., Talbot, C.J., Koyi, H.A., 2010. Viscosity estimates of salt in the Hormuz and Namakdan salt diapirs, Persian Gulf. Geol. Mag. 147, 497–507.
Nikolinakou, M.A., Flemings, P.B., Hudec, M.R., 2014. Modeling stress evolution around a rising salt diapir. Mar. Petrol. Geol. 51, 230–238.
Nilsen, K.T., Vendeville, B.C., Johansen, J.T., 1995. Influence of regional tectonics on halokinesis in the nordkapp basin, barents sea. In: Jackson, M.P.A., Roberts, D.G., Snelson, S. (Eds.), Salt Tectonics: A Global Perspective, vol. 65. American Association of Petroleum Geologists Memoir, Tulsa, OK, pp. 413–436.
NIOC, 2004a. Geological Map at 1:100,000 Scale. Sheet 20874E (Gavbast). National Iranian Oil Company.
NIOC, 2004b. Geological Map at 1:100,000 Scale. Sheet 42993 (Lamazan). National Iranian Oil Company.
Nissen, E., Tatar, M., Jackson, J.A., Allen, M.B., 2011. New views on earthquake faulting in the Zagros fold-and-thrust belt of Iran. Geophys. J. Int. 186, 928–944.
Owen, P.F., Taylor, N.G., 1983. A salt pillow structure in the southern North Sea. In: Bally, A.W. (Ed.), Seismic Expressions of Structural Styles; a Picture and Work Atlas, vol. 15. AAPG, Studies in Geology series, 2.3.2-7 - 2.3.2-10.
Perry, J.T.O.'.B., Setudehnia, A., Nars, M., 1965. South-East Fars Geological Compilation Map at 1:250,000. Iranian Oil Operating Companies. Geological and Exploration Division, Tehran.
Parker, T.J., McDowell, A.N., 1951. Scale models as guide to interpretation of salt-dome faulting. AAPG (Am. Assoc. Pet. Geol.) Bull. 35, 2076–2086.
Parker, T.J., McDowell, A.N., 1955. Model studies of salt-dome tectonics. AAPG (Am. Assoc. Pet. Geol.) Bull. 39, 2384–2470.
Ruh, J.B., Hirt, A.M., Burg, J.P., Mohammadi, A., 2014. Forward propagation of the Zagros Simply Folded Belt constrained from magnetostratigraphy of growth strata. Tectonics 33, 1534–1551.
Schmidtz, J., Flizeder, F., 1993. Structure of a classic chalk oil field and production enhancement by horizontal drilling, Reitbrook, NW Germany. In: Spencer, A.M. (Ed.), Generation, Accumulation and Production of Europe's Hydrocarbons III, vol. 3. European Association of Petroleum Geoscientists Special Publication, pp. 144–154.
Schultz-Ela, D.D., Jackson, M.P.A., Vendeville, B.C., 1993. Mechanics of active salt diapirism. Tectonophysics 228, 275–312.
Sepehr, M., Cosgrove, J.W., 2004. Structural framework of the Zagros fold–thrust belt, Iran. Mar. Petrol. Geol. 21, 829–843.
Sims, D.W., Morris, A.P., Wyrick, D.Y., Ferrill, D.A., Waiting, D.J., Franklin, N.M., Colton, S.L., Umezawa, Y.T., Takanashi, M., Beverly, E.J., 2013. Analog modeling of normal faulting above Middle East domes during regional extension. AAPG (Am. Assoc. Pet. Geol.) Bull. 97, 877–898.
Snidero, M., Muñoz, J.A., Carrera, N., Butillé, M., Mencos, J., Motamedi, H., Piryaei, A., Sàbat, F., 2019. Temporal evolution of the Darmadan salt diapir, eastern Fars region, Iran. Tectonophysics 766, 115–130.
Stewart, S.A., 2006. Implications of passive salt diapir kinematics for reservoir segmentation by radial and concentric faults. Mar. Petrol. Geol. 23, 843–853.
Stöklin, J., 1968. Structural history and tectonics of Iran: a review. Am. Assoc. Petroelum Geol. Bulletin 52, 1229–1258.
Talbot, C.J., Alavi, M., 1996. The Past of a Future Syntaxis across the Zagros, vol. 100. Geological Society, London, Special Publication, pp. 89–109.
Talbot, C.J., Pohjola, V., 2009. Subaerial salt extrusions in Iran as analogues of ice sheets, streams and glaciers. Earth Sci. Rev. 97, 155–183.
Talebian, M., Jackson, J., 2004. A reappraisal of earthquake focal mechanisms and active shortening in the Zagros mountains of Iran. Geophys. J. Int. 156, 506–526.
Tavakoli, F., Walpersdorf, A., Authemayou, C., Nankali, H.R., Hatzfeld, D., Tatar, M., Djamour, Y., Nilforoushan, F., Cotte, N., 2008. Distribution of the right-lateral strike–slip motion from the main recent fault to the Kazerun Fault System (Zagros, Iran): evidence from present-day GPS velocities. Earth Planet Sci. Lett. 275, 342–347.
Tsou, C.Y., Feng, Z.Y., Chigira, M., 2011. Catastrophic landslide induced by typhoon morakot, Shiaolin, taiwan. Geomorphology 127, 166–178.
Vernant, P., Nilforoushan, F., Hatzfeld, D., Abbassi, M.R., Vigny, C., Masson, F., Nankali, H., Martinod, J., Ashtiani, A., Bayer, R., Tavakoli, F., Chéry, J., 2004. Present-day crustal deformation and plate kinematics in the Middle East constrained by GPS measurements in Iran and northern Oman. Geophys. J. Int. 157, 381–398.
Vendeville, B.C., Nilsen, K.T., 1995. Episodic growth of salt diapirs driven by horizontal shortening. In: Salt, Sediment and Hydrocarbons. Society of Economic Paleontologists and Mineralogists Gulf Coast Section. 16th Annual Research Conference Program and Extended Abstracts, pp. 285–295.
Vergés, J., Emami, H., Garcés, M., Beamud, E., Homke, S., Skott, P., 2019. Zagros foreland fold belt timing across Lurestan to constrain Arabia-Iran collision. In: Saein, A.F. (Ed.), Developments in Structural Geology and Tectonics, vol. 3. Elsevier, Amsterdam, pp. 29–52.
Walker, R.T., Andalibi, M.J., Gheitanchi, M.R., Jackson, J.A., Karegar, S., Priestley, K., 2005. Seismological and field observations from the 1990 November 6 Furg (Hormozgan) earthquake: a rare case of surface rupture in the Zagros mountains of Iran. Geophys. J. Int. 163, 567–579.
Walker, R.T., Khatib, M.M., Bahroudi, A., Rodés, A., Schnabel, C., Fattahi, M., Talebian, M., Bergman, E., 2015. Co-seismic, geomorphic, and geologic fold growth associated with the 1978 Tabas-e-Golshan earthquake fault in eastern Iran. Geomorphology 237, 98–118.
Walpersdorf, A., Hatzfeld, D., Nankali, H., Tavakoli, F., Nilforoushan, F., Tatar, M., Vernant, P., Chéry, J., Masson, F., 2006. Difference in the GPS deformation pattern of north and central Zagros (Iran). Geophys. J. Int. 167, 1077–1088.
Wessel, B., 2016. TanDEM-X Ground Segment – DEM Products Specification Document. EOC, DLR, Oberpfaffenhofen, Germany, Public Document TD-GS-PS-0021, Issue 3.2, 2016. Available: https://tandemx-science.dlr.de/.
Withjack, M.O., Scheiner, C., 1982. Fault patterns associated with domes—an experimental and analytical study. AAPG (Am. Assoc. Pet. Geol.) Bull. 66, 302–316.
Yin, H., Groshong, R.H., 2007. A three-dimensional kinematic model for the deformation above an active diapir. AAPG (Am. Assoc. Pet. Geol.) Bull. 91, 343–363.
Zarei, M., Raeisi, E., Talbot, C., 2012. Karst development on a mobile substrate: konarsiah salt extrusion, Iran. Geol. Mag. 149, 412–422.
Závada, P., Bruthans, J., Adineh, S., Warsitzka, M., Zare, M., 2021. Composition and deformation patterns of the caprock on salt extrusions in southern Iran. Filed study on the Karmostaj and Siah Taq diapirs. Jorunal of Structural Geology 151, 104422.
Zhao, S., Chigira, M., Wu, X., 2018. Buckling deformations at the 2017 Xinmo landslide site and nearby slopes. Maoxian, Sichuan, Chine, Engineering Geology 2018, 187–197.